Kindling Dravet Syndrome Symptoms from the Hippocampus

Rachael Stein

A dissertation

submitted in partial fulfillment of the

requirements for the degree of

Doctor of Philosophy

University of Washington

2019

Reading Committee:

William Catterall, Chair

Gwenn Garden

Larry Zweifel

Program Authorized to Offer Degree:

Neuroscience

University of Washington

Abstract

Kindling Dravet Syndrome Symptoms from the Hippocampus

Rachael Stein

Chair of the Supervisory Committee:

William Catterall

Department of Pharmacology

Dravet Syndrome is an epileptic condition with varied comorbidities caused by haploinsufficiency of the *Scn1a* gene, which encodes the alpha-1 subunit of the $Na_V1.1$ sodium channel. Dravet Syndrome is characterized by treatment-refractory epileptic seizures that present at an early age, followed by other comorbidities such as autism and cognitive impairment. The mouse model of Dravet Syndrome closely mirrors the mutations and phenotypes present in the human population, which result from hypoexcitability of forebrain GABAergic interneuron populations due to reduced sodium current after loss-of-function in $Na_V1.1$ channels. However, the region-specific impact of reduced Nav1.1 expression on epileptiform activity and Dravet symptoms has been unknown. We hypothesized that decreased interneuron activity which results in increased excitability and dysregulation in distinct and varied brain regions is responsible for the phenotypes of Dravet Syndrome. Through a series of genetic, physiological, and behavioral experiments, we have identified the hippocampus as a critical region in which loss-of-function of Nav1.1 channels contributes to the symptoms of Dravet Syndrome. These studies have increased our understanding of the molecular mechanisms behind the disease and has revealed anatomical targets for pharmacological management.

Table of Contents

Acknowledgments

I'd like to dedicate this thesis to my parents, Bea and Larry, who nurtured my love of science from an early age and have always encouraged me to pursue my dreams. I could not have gotten this far without their encouragement, love, and dedication.

I'd also like to acknowledge the support I've received from my family, friends and mentors, both within and outside of the University of Washington, for helping me make the most of my time in graduate school and prepare for my career ahead. Specifically, I'd like to recognize my advisor, Dr. William Catterall, for giving me the structure and guidance needed to complete my dissertation while allowing me the flexibility to foster my scientific interests both inside and outside the lab.

Chapter 1: Introduction

1.1 History of Epilepsy

Brain activity occurs in the form of electrical discharges from connected neuron populations. In a normally functioning brain, excitation and inhibition of various neural populations are kept at some internal balance point. However, when this balance is upset either due to increased excitation, decreased inhibition, or both, the brain can tip into a hyperexcitable state known as epilepsy. The word "epilepsy" is derived from the Greek word "epilepsia", which translates to "to take hold of", and the symptoms manifest themselves as seizures, or abnormal or synchronized electrical discharges. These seizures can be partial seizures, which are confined to one brain region or generalized seizures, where abnormal activity spreads throughout the brain (Engel, 1996).

Recorded incidences of epilepsy have been traced all the way to Babylonian tablets created around 2000 BC, which depict many different types of seizures and attributes each type to a specific deity, therefore relegating its treatment as a spiritual matter. This ultimately gave rise to the Greek 5th century view of epilepsy as the "Sacred Disease", a theorem reflected in Hippocrates' text by the same name. However, Hippocrates argued that that the symptoms of the disease were not divine phenomena, but rather a medical condition affecting the brain (Temkin, 1945). Unfortunately, this view wasn't made popular until the late 18th/early 19th century, and until then, the disease was largely treated as a supernatural affliction, treated with everything from trepanation to exorcisms (Luders, 2008) . After the emergence of the distinct field of neuroscience in the mid-1800s, the first effective anti-seizure medication, bromide, was introduced and became widely used in the ensuing decades (Pearce, 2002). Further steps towards understanding the disease were made with the development of the EEG system by Hans Berger in the 1920s, which confirmed the presence of abnormal electrical activity and allowed doctors and scientists to further classify seizure types

based on waveform activity as well as to localize seizure foci, which expanded their ability to treat the disease with neurosurgery (Engel, 1990). Since then, scientific discoveries, especially those concerning neuronal electrochemical excitability, and innovations in functional neuroimaging have facilitated many modern pharmacological treatments for epilepsy. However, treatment success varies based on the origin and cause of the disease (Gschwind and Seeck, 2016).

1.2 Types of Epilepsies

Epileptic seizures themselves can be classified according to origin, type of onset, and regions affected. The International League Against Epilepsy's (ILAE) 2017 classification scheme subdivides seizure types into those which have a focal vs generalized onset, and then further distinguishes between motor and non-motor seizures, and whether the patient is awake or experiences impaired consciousness (Fisher et al., 2017).

There are many perturbations to the brain which can cause epilepsy. These causes are often multifactorial and can include environmental, acquired, and genetic components. Brain trauma, stroke, infection, substance abuse, and autoimmune dysfunction can all result in repeated seizures, and the advent of modern sequencing has started to identify genetic factors which were previously labeled as idiopathic. In many cases in which a genetic component has been identified, the genes involved often affect ion channels, which gate excitability, either directly or indirectly (Shorvon S et al., 2019).

1.3 Dravet Syndrome

Origin and epidemiology

One such type of genetic epilepsy is Dravet Syndrome. Dravet Syndrome was first documented and described in 1978 in France, and recognized as a syndrome in 1989. Originally called "Severe

Myoclonic Epilepsy of Infancy", its name was changed to "Dravet Syndrome" to more fully encompass its symptoms as some of the patients did not have myoclonus and the symptoms persist into adulthood (Dravet, 2011a). Dravet Syndrome is a relatively rare disease, affecting less than one person out of 21,000 live births as measured in the United States (Dravet, 2011b).

Symptoms usually present in the first year of life with a seizure, often triggered by a fever or immersion in hot water, both of which result in body temperature elevation. These seizures progress until they are both febrile and spontaneously occurring and accompany gait deficiencies and developmental delays. Dravet Syndrome has a significantly higher mortality rate than other types of epilepsies. A recent study that followed 100 Dravet patients found that the Dravet-specific mortality rate was 15.8 percent, at a median age of seven years. Of these deaths, ten were from SUDEP, or sudden unexpected death in epilepsy, and four were from status epilepticus (prolonged continuous seizures). This SUDEP rate is significantly higher than those of other epileptic disorders, and largely occurs during childhood. (Cooper et al., 2016). However, studies of Dravet patients in adulthood still demonstrate significant mortality. As an epileptic condition, Dravet Syndrome is unique due to its many associated co-morbidities. Accompanying the seizures are severe cognitive deficits, autistic behavior, circadian deficits, and hyperactivity which persist into adulthood. In addition to the seizures, the frequency of which general decrease if the patient reaches adulthood, these co-morbidities greatly reduce quality of life. In a recent survey of twenty-four Dravet patients, only 3 were able to live independently without assistance (Genton et al., 2011).

Etiology

A majority of Dravet patients (>80%) have been found to have defects in the *SCN1A* gene, which encodes the alpha pore-forming subunit of the voltage gated sodium channel $Na_V1.1$ (Claes et al.,

2003) . Sodium channels are largely responsible for propagating action potentials in most cells that are electrically excitable. The alpha subunits of voltage gated sodium channels are composed of four homologous domains comprised of six helical transmembrane segments (S1-S6). Their functionality is controlled by the pore region and positively charged selectivity filter, which mediates the flow of negatively charged sodium ions through the channel, and by the voltage sensor, which activates the channel in response to membrane depolarization. These alpha subunits are usually associated with one or more beta subunits, which are comprised of an extracellular immunoglobulin-like domain, a single transmembrane segment, and a short intracellular domain. The beta subunits help to localize the channel within the membrane (Catterall, 2000).

$Na_V1.1$ is mostly localized to the cell body and axon initial segment, which is expected given its role in propagation of the action potential (Ogiwara et al., 2007; Trimmer, 1998; Westenbroek et al., 1989; Yu et al., 2006). The severity of the disease symptoms exists on a spectrum which is largely correlated with the functionality of the $Na_V1.1$ channel; as the functionality decreases, the symptoms become more and more severe. Mild missense mutations in the *SCN1A* gene can cause febrile seizures, while moderate to severe missense mutations often result in Generalized Epilepsy with Febrile Seizures plus (GEFS+) (Catterall et al., 2010b). Dravet Syndrome is the most severe, with complete heterozygous loss of function in the channel and a host of other comorbidities (Catterall, 2014). There are hundreds of different mutations that have been identified in the *SCN1A* gene which can lead to Dravet Syndrome, and although most mutations are de novo in nature, about 5-10% of cases arise from familial mutations (Marini et al., 2011). Within these familial mutations, the same mutation can result in symptoms of varied severity; some affected members have mild or no epileptic phenotype while others are severely affected (Nabbout et al., 2003).

These differences in disease severity for patients with the same mutation suggest that there are strong effects of genetic background in Dravet Syndrome.

Cell type specific responses to Scn1a deletion

Even though the mutations which cause Dravet Syndrome aren't limited to specific cell types and are present throughout the entire body, studies have shown that some cell types are more affected than others by this mutation. One such affected population are inhibitory, GABAergic interneurons. Although they only compromise about 10-20% of cortical and other associated neuronal populations, compared to excitatory neuronal subtypes, GABAergic inhibitory interneurons serve many valuable roles throughout the brain. They are electrically, morphologically, and transcriptionally diverse, and their inhibitory activity is critically important in setting the pace, gain, and patterns of excitatory pyramidal cell activity (Crandall and Connors, 2016).

Although it is estimated that there are over 20 subtypes of GABAergic interneurons, they can be largely divided into three groups based on their expression of the calcium binding protein parvalbumin, the neuropeptide somatostatin, or serotonin receptor 5HT3aR (Rudy et al., 2011).

During development and embryogenesis, these differently fated populations of GABAergic neurons are largely generated in the ganglionic eminence (GE), located in the ventral area of the telencephalon. The GE is subdivided into the medial ganglionic eminence (MGE), the caudal ganglionic eminence (CGE), and the lateral ganglionic eminence (LGE). The MGE is the origin of about 50-60% of the GABAergic cortical interneurons and gives rise to most of the SST and PV populations. The CGE produces about 30-40% of cortical GABAergic interneurons and is the second largest source of interneuron progenitors, producing largely 5HT3aR expressing

GABAergic neurons (Kelsom and Lu, 2013). Studies have also implicated the embryonic preoptic area (POA), a region of the hypothalamus, as another source of perhaps 10% of the GABAergic interneurons in the cortex (Gelman et al., 2011). Transcription factors, such as the *Dlx* genes, serve an important role in guiding these cells to their final destination (Manent et al., 2011).

Although the global mutation is not cell specific and $Na_V1.1$ is expressed throughout the brain, reduced sodium current is observed specifically in hippocampal, cortical, and cerebellar GABAergic inhibitory interneurons (Catterall et al., 2010a; Han et al., 2012a; Hedrich et al., 2014; Ogiwara et al., 2007; Yu et al., 2006). Interestingly, while reduced sodium current in inhibitory interneurons is observed across all mouse models of Dravet Syndrome, there is some conflicting evidence as to the response of excitatory neurons as a result of *Scn1a* mutation. Several studies (Oakley et al., 2009; Ogiwara et al., 2013; Tai et al., 2014; Yu et al., 2006) observe no appreciable decrease of sodium current or electrical excitability in excitatory neurons, while another study finds an age-dependent increase in sodium current in excitatory neurons in a different genetic background (Mistry et al., 2014). These varied results could be the result of compensatory conduction through other ion channels which are not as highly expressed in interneurons, or through some other mechanism yet undiscovered which varies between disease models. However, the consistent decreased excitability in inhibitory cell populations is likely the cause of the ataxia and seizure activity seen in the affected human and mouse populations (Kalume et al., 2007; Oakley et al., 2009; Ogiwara et al., 2013; Tai et al., 2014; Yu et al., 2006). Indeed, deletion of *Scn1a* in only forebrain interneuron populations utilizing a Cre-Lox methodology and the *Dlx1,2* enhancer is both necessary and sufficient to induce seizures and premature death with the same severity as the global deletion (Cheah et al., 2012; Ito et al., 2013a; Tatsukawa et al., 2018a). In one study, deletion of $Na_V1.1$ in excitatory neuron populations ameliorates some of the epileptic

seizures and indicates that excitatory neurons may also play a role in the *Scn1a* mutation phenotype (Ogiwara et al., 2013). Thus, multiple studies have demonstrated cell-specific effects of *Scn1a* mutations on inhibitory vs. excitatory neurons; however, the underlying mechanisms are not clear. One hypothesis is that inhibitory interneurons express $Na_V1.1$ at higher levels than other sodium channel types compared to excitatory neurons in which they are a minority of sodium channels. While this has been reported, the total sodium current density is also lower in excitatory neurons, and thus lower expression of $Na_V1.1$ in excitatory cells might not translate into a lower ratio of $Na_V1.1$ compared to all sodium channels (Mistry et al., 2014). Regardless of the underlying cause, it remains vitally important to dissect the cell-type specific and regional contributions to the symptoms of Dravet Syndrome.

Current treatments for Dravet Syndrome

Pharmacological management of the disorder has met with little success; most treatment plans focus on preventing recurrence of seizure activity and do not alleviate the accompanying cognitive and behavioral impairments (Chiron and Dulac, 2011). In addition, many traditional anti-epileptics such as carbamazepine or phenytoin, which act on sodium channels, can actually exacerbate seizure frequency and severity in patients with Dravet Syndrome (Hawkins et al., 2017). Currently, many patients are treated with a combination of anti-epileptic drugs (including clonazepam, valproate, topiramate, and stiripentol) and lifestyle modifications, such as the ketogenic diet (Chiron and Dulac, 2011) . Recently, there has been reported success in treating seizures with cannabidiol (CBD), which in mice increases the amount of inhibitory neurotransmission and alleviates the severity of seizures and social deficits (Devinsky et al., 2017; Kaplan et al., 2017; Leo et al., 2016). In addition, Petrou et al demonstrated success in reducing seizure severity and increasing sodium currents only in Dravet Syndrome mice with the use of a $Na_V1.1$ activating

compound, δ-theraphotoxin-Hm1a (Hm1a), which is a peptide toxin derived from the venom of a tarantula (Richards et al., 2018). However, a major caveat to this treatment is that the toxin activates sodium channels throughout the body, and isn't confined to the brain, which could lead to unwanted side effects such as pain or cardiac arrhythmia. Recently, the emergence of RNA therapies and other gene modifying treatments presents a plethora of new potential therapies, but there is significant risk associated with direct genetic upregulation and modification, the full effects of which might not be realized for years. Therefore, ascertaining the minimal dose or treatment area of these novel therapeutics could be very important to minimizing these issues.

1.4 Thesis Aim

Even with modern DNA sequencing and imaging techniques, it's unknown which brain regions are affected by *Scn1a* deficiency to contribute to epileptic activity and behavioral comorbidities. We know that in Dravet Syndrome, hypoactivity of interneuron populations has been observed in many regions of the brain, and we can therefore hypothesize that this hypoactivity of inhibitory cell populations in specific brain regions could lead to the varied symptoms of the disease. However, so far these studies have been correlative instead of causative. Using genetic and viral manipulations, we sought to identify and attribute the contributions of various brain regions to the hyperexcitability and symptoms associated with Dravet Syndrome after local or global loss of $Na_V1.1$. Our findings expand the knowledge of the pathophysiology of Dravet Syndrome and reveal regions of the brain which could be specifically targeted with therapeutics to reduce off target effects.

Chapter 2: Discerning the Loci of Increased Neural Activity in Murine Dravet Syndrome

2.1 Abstract

Dravet Syndrome is an epileptic condition with stereotyped comorbidities caused by haploinsufficiency of the sodium channel Nav1.1 as a result of mutations in the *SCN1A* gene. Symptoms such as seizures, cognitive defects, and autistic characteristics manifest themselves at an early age, and are poorly controlled by current pharmacological compounds. The mouse model of Dravet Syndrome closely genocopies and phenocopies the human disorder. These mice experience thermally induced seizures starting at P21, even though electrophysiological deficits are observed as early as P14. We asked if we could observe local areas of hyperexcitability in *Scn1a*$^{+/-}$ mice in the days preceding epileptic activity using the Fos TRAP system, in which cells active during a 12-hour period are permanently stained with a tdTomato reporter gene whose expression is controlled in an activity-dependent way by the constitutively active CBA promoter. Although we observed no local areas of hyperexcitability at any of the time points leading up to the period of epileptic susceptibility, thermal induction of seizure activity generated hyperexcitability in the cortex and specific activation of the dentate gyrus and lateral CA2/CA3 regions of the hippocampus. These findings implicate the hippocampus, specifically the dentate gyrus, as potentially important in the initiation and propagation of epileptic activity in the Dravet Syndrome mouse.

2.2 Introduction

Dravet Syndrome, also known as Severe Myoclonic Epilepsy of Infancy (SMEI), was first described in 1978 and is characterized by increasingly severe epileptic symptoms occurring in

previously healthy children, usually under the age of one. Multiple comorbidities accompany the disease including cognitive and social impairments, hyperactivity, and circadian defects (Dravet, 2011a). The molecular etiology has been largely elucidated, with 70-80% of patients displaying haploinsufficiency due to a loss-of-function mutation in the sodium channel alpha-1 subunit (*SCN1A*) gene, which encodes the pore-forming subunit in the voltage-gated sodium channel NaV1.1 (Catterall, 2018; Claes et al., 2003; Claes et al., 2001; Marini et al., 2011). In mice, expression of *Scn1a* is localized to the neuronal cell bodies and initial segments and rapidly increases after the second week of life. *Scn1a* heterozygotes (+/-) both genocopy and phenocopy the human syndrome. They have spontaneous seizures, cognitive and social impairments, ataxia at a young age, and are at increased risk of SUDEP. In addition, all mice demonstrate generalized tonic seizures when their body temperatures are elevated, which is consistent with early febrile seizures in Dravet Syndrome patients. Although the global mutation is not cell-specific, reduced sodium current has been observed specifically in GABAergic inhibitory neurons in the hippocampus, cortex, thalamus, and cerebellum (Kalume et al., 2015; Kalume et al., 2007; Ogiwara et al., 2007; Tai et al., 2014; Yu et al., 2006). Interestingly, deletion of *Scn1a* in excitatory pyramidal cells yields no appreciable sodium current decrease; this is probably due to lower levels of *Scn1a* expression or compensatory up-regulation of other sodium channel isoforms (Ogiwara et al., 2013; Schutte et al., 2016; Yu et al., 2006). Specific deletion of *Scn1a* in forebrain interneurons utilizing the Cre-Lox methodology and the *Dlx1,2* enhancer is both necessary and sufficient to induce the core Dravet Syndrome phenotypes of premature death, seizures, autistic-like behavior, and cognitive deficits (Cheah et al., 2012; Han et al., 2012a; Kalume et al., 2015). These results suggest that selective hypoexcitability of inhibitory cells cause seizure activity and some of the behavioral impairments seen in the affected human and mouse populations (Oakley et al., 2009;

Rubinstein et al., 2015a; Tai et al., 2014; Tatsukawa et al., 2018a; Yu et al., 2006). Children with Dravet Syndrome do not start having seizures until they are six months or more old, suggesting an age-dependent susceptibility; often the first set of epileptic activity is triggered by a fever or hot bath, which increases body temperature. In addition, seizure severity also increases with age (Dravet, 2011b). Similarly, in the Dravet Syndrome mouse model, animals are resistant to thermally induced seizures until P20, and do not exhibit spontaneous seizure activity until several days later, the severity of which increases with age (Oakley et al., 2009). This is interesting given that electrophysiological recordings demonstrate reduced sodium current specifically within GABAergic interneurons as early as P14, a period in which $Na_V1.1$ is increasing in the brain while expression of $Na_V1.3$, another sodium channel, is decreasing (Cheah et al., 2013; Yu et al., 2006).

Little is known about how these early impairments in GABAergic cell firing eventually lead to propagation and induction of seizure activity. This period of sensitization in other models is known as epileptogenesis, or the process by which a normally functioning brain develops epilepsy. In the pilocarpine model of temporal lobe seizures, epileptogenesis occurs after animals are exposed to doses of pilocarpine hydrochloride, which acts as a cholinergic muscarinic agonist. In this model, the period of epileptogenesis is characterized by a variety of neurological and structural changes, including upregulation of cellular T-type Ca2+ currents, which result in increased action potential firing (Becker et al., 2008). Thus, by examining overall neural activity in Dravet Syndrome animals during the transitory period between an observable defect in inhibitory cell activity and the eventual propagation of abnormal neural excitation, we could reveal loci of abnormal activity well as targets for pharmacological intervention. We hypothesized that regions of hyperexcitability would emerge before spontaneous seizures were generated, and we expected that these regions of hyperexcitability might drive development of the epileptic phenotype. In order to map activity

patterns over the course of epileptic development, we used the TRAP methodology in which active cells are permanently labeled with a fluorescent reporter, to evaluate regions of activity during a time course of *Fos2a Scn1a* heterozygous and *Fos2a* WT mouse development.

2.3 Keywords

Nav1.1, *Scn1a*, TRAP, *cFos*, Dravet

2.4 Results

4-Hydroxytamoxifen injection into Fos2a/Scn1a mice results in robust tdTomato reporter expression

To visualize neural activity "trapped" in a period of time, we utilized the Fos2a-TRAP mouse line, in which tamoxifen-dependent Cre recombinase ($CreER^{T2}$) is expressed in an activity-dependent manner under the intermediate early gene (IEG) c-Fos. Quiescent cells express low levels of IEGs, but IEG expression can be induced rapidly and transiently by neural activity (Sheng and Greenberg, 1990). Therefore, an increase in c-Fos staining indicates enhanced excitatory neural activity. In this model, active c-Fos-transcribing cells express $CreER^{T2}$, which goes on to induce expression of a fluorescent reporter gene only in the presence of 4-hydroxytamoxifen, which allows visualization of active cell populations during a time window of less than 12 hrs (Guenthner et al., 2013) (Fig. 1A). By breeding these animals with our heterozygous *Scn1a* knock-out animals ($Scn1a^{+/-}$, or "HET"), we were able to compare patterns of activity between *Fos2a* wild type (WT) ($Fos2a^{+/-}$, $TdTomato^{+/-}$,*Scn1a* WT) and *Fos2a* $Scn1a^{+/-}$ ($Fos2a^{+/-}$, $TdTomato^{+/-}$,$Scn1a^{+/-}$) animals in a temporally controlled fashion. To ensure that tdTomato expression was specifically activated by tamoxifen, we first injected animals with vehicle alone, and did not observe any inappropriate reporter expression after two weeks (Fig.1B). However, 4-hydroxytamoxifen induced robust reporter expression in both *Fos2a* WT and Fos2a $Scn1a^{+/-}$ animals (Fig. 1B).

Fos2a Scn1a$^{+/-}$ animals do not display specific loci of hyperactivity during epileptogeneis

In order to observe a visual time course of active cell populations in the developing Dravet Syndrome mice compared to their WT littermates, we first injected separate mouse cohorts of *Fos2a* WT and *Fos2a Scn1a*$^{+/-}$ animals on sequential days starting at P16, when the animals display defects in GABAergic neuronal firing but are not epileptic, and ending at P21, after the animals are susceptible to thermally evoked seizures. Injected cohorts of male and female animals were allowed to age for two weeks, and then perfused and assayed for reporter expression at ages P30-P35 (Fig. 1C).

We observed no consistent visual difference in tdTomato reporter expression between WT and *Scn1a+/-* mice at any of the six age points (P16-P21) that we studied. While we noted general electrical activity present in many brain regions, no individual regions we observed were visually different between the two cohorts. We quantified cell bodies in several regions where generalized electrical activity in both groups was observed, including the visual cortex, somatosensory cortex, and thalamic regions, and noticed no significant differences between the two genotypes (Fig. 2A-C).

Because of its demonstrated role in epilepsy, and previous studies showing that the largest impairments in excitability are found within hippocampal interneurons (Bechi et al., 2012; Yu et al., 2006), we additionally counted tdTomato+ cells within the hippocampus. Because the hippocampus is such a large, curved structure, it can be broadly divided up by sub-regions (dentate gyrus, CA2/3, and CA1), as well as its location in brain (the dorsal-medial and ventral-lateral components). Therefore, we counted cell bodies from three regions (the dentate gyrus, CA3/CA2, and CA1) of both the dorsal-medial and ventral lateral hippocampus. Similarly, we did not observe

any significant differences in tdTomato+ cell number between WT and *Scn1a*$^{+/-}$ mice in any of the regions or ages (Fig. 3).

Thermal induction of epileptic activity causes generalized excitability and specific activation of the dentate gyrus.

As the first seizures in children affected by Dravet Syndrome usually present following exposure to a thermal stimulus such as a fever or hot bath, triggering thermal seizures in Dravet Syndrome mice provides an inducible epileptic correlate in the mouse model (Dravet et al., 2005; Oakley et al., 2009). We sought to characterize the excitability of different brain regions upon seizure induction. *Fos2a Scn1a*$^{+/-}$ mice and their wild type littermates were injected at P23/P24 with 4-hydroxytamoxifen and thermally induced 2-4 hours after injection (Reid et al., 2014). During the thermal induction paradigm, mice are contained in a small chamber and their internal body temperature is raised 0.5º C every two minutes from 36.5ºC until 41ºC or until the animal has a seizure. This process, conducted using an internal temperature probe connected to a heat lamp, simulates the gradual rise in body temperature during a fever, which trigger seizures in Dravet Syndrome patients. While none of the *Fos2a* WT induced animals experienced epileptic activity during the thermal induction process, all *Fos2a Scn1a*$^{+/-}$ induced mice experienced Racine 4/5 generalized seizures. In order to control for baseline activity, we also injected 4-hydroxytamoxifen in *Fos2a* WT control and *Fos2a Scn1a*$^{+/-}$ control animals which underwent the same paradigm minus the heating element. All cohorts of animals were aged for two weeks after induction, perfused and imaged. While we observed no difference in activity between the control *Fos2a* WT and control *Fos2a Scn1a*$^{+/-}$ animals, we generally observed increases in neuronal activity by counting cell bodies in cortical regions of thermally induced *Fos2a Scn1a*$^{+/-}$ mice, including the somatosensory cortex (*Fos2a* WT: Mean = 491± 114, N = 6; *Fos2a Scn1a*$^{+/-}$ Mean = 891 ± 135.7, n=6; P = 0.0479) and the visual cortex (*Fos2a* WT: Mean = 657 ± 78.4, n=6; *Fos2a Scn1a*$^{+/-}$

Mean = 1329 ± 191, n=6; P = 0.0086) (Fig. 4 A-E). There was no difference in number of tdTomato cell bodies between the induced cohorts when measured in the thalamic regions.

Interestingly, the most striking difference between the two induced cohorts of mice came from within the hippocampus. We counted tdTomato+ cells from three regions (dentate gyrus, CA2/3, CA1) within the dorsal medial and ventral lateral regions of the structure. While *Fos2a* WT induced animals displayed low levels of hippocampal activity, *Fos2a Scn1a*$^{+/-}$ induced mice showed significantly increased levels of tdTomato+ cells within the hippocampal structure (Fig. 5A-B). The largest hippocampal differences between the induced *Fos2a* WT and *Fos2a Scn1a*$^{+/-}$ (Fig. 5 B-C) were found in the dorsal (*Fos2a* WT: Mean =16.5 ± 2.20, n=6; *Fos2a Scn1a*$^{+/-}$ Mean: 198 ± 35.3, n=6; P = 0.0005) and lateral (*Fos2a* WT: Mean =13.2 ± 1.32, n=6; *Fos2a Scn1a*$^{+/-}$ Mean: 145 ± 23, n=6; P = 0.0002) dentate gyrus of the hippocampus. The Ca2/3 region of the lateral hippocampus also displayed increased expression in the *Fos2a Scn1a*$^{+/-}$ mice (Fos2a WT: Mean = 25.83 ± 2.676, n=6; *Fos2a Scn1a*$^{+/-}$ Mean: 52.5 ± 3.836, n=6; P = 0.0002) (Fig 5C). These results point to the hippocampus as a major driver of seizure activity in response to thermal stimulation in Dravet Syndrome mice.

2.5 Discussion

Hyperexcitability in Dravet Syndrome mice during epileptogenesis

Epileptogenesis is the process by which a previously normal neuronal network is somehow altered to become predisposed to epileptic activity. This process can occur during a "latent" period, where the brain has experienced or been exposed to an epileptogenic trigger but before the first clinical seizure begins. In Dravet Syndrome mice, even though there is electrophysiological impairment of various interneuron populations at P14, *Scn1a*$^{+/-}$mice are not susceptible to thermally induced

seizures until P21. Using the *c-fos* TRAP methodology, we wanted to identify the development of discrete loci of hyperexcitability during this period. However, surprisingly, we did not observe any changes in neuronal activity between WT and *Scn1a*$^{+/-}$ mice during the period from P16 and P21.

This finding could indicate either that there are no detectable discrete regions of hyperactivity during the period of epileptogenesis in Dravet Syndrome mice or that electrical activity in such regions is below the threshold level for detection by the *c-Fos* TRAP methodology. While the TRAP technique was sensitive enough to capture gross excitability due to a seizure, it is possible that there is a threshold of activity needed to trigger reporter expression, which was not reached in pre-seizure hyperactivity.

Hippocampal role during thermally induced seizures

While prior research has been conducted examining *c-Fos* expression at designated time points after seizure activity, most of these studies have induced epileptic activity using chemoconvulsants or lesion-based models. We sought to capture a much larger "window" of activity using the TRAP methodology, in a mouse model where seizures can be induced by a pathophysiologically relevant stimulus instead of a chemoconvulsant.

We were not surprised to see generalized increases in cortical activation after thermal induction, as all induced *Fos2a Scn1a*$^{+/-}$ mice experienced generalized tonic-clonic seizures that propagate throughout the entire brain. Previous research in other mouse models has demonstrated increased cortical activity after chemically induced seizures, as well as a lack of increased excitability in regions such as the thalamus (Yu et al., 2016).

Our results confirm the importance of the hippocampus in the initiation of epileptic activity. Previous research has shown that repeated stimulation of the hippocampus can induce generalized

epilepsy (Lothman et al., 1992) and that optogenetic manipulation of dentate gyrus granule cells is sufficient to induce epilepsy in previously healthy mice (Krook-Magnuson et al., 2015; Krook-Magnuson et al., 2014). Moreover, hippocampal interneurons have the largest loss of sodium current in Dravet Syndrome mice (Catterall et al., 2010a; Han et al., 2012a; Hedrich et al., 2014; Ogiwara et al., 2007; Yu et al., 2006). Interestingly, we found that the dentate gyrus showed the largest difference between WT and *Scna1*$^{+/-}$ within the hippocampus as a whole, and especially within the dorsal hippocampus. Previous research has shown that *c-Fos* expression increases in the hippocampus following seizures induced by chemoconvulsants, although this activity is not specific only to the dentate gyrus (Yang et al., 2019; Yu et al., 2016). Therefore, the activation of the hippocampal regions points to a role of the hippocampus, and especially the dentate gyrus, in the propagation or initiation of Dravet Syndrome seizures.

2.6 Methods

All experiments were carried out in C57BL/6J mouse genetic background. Experiments were performed according to guidelines established in the National Institutes of Health Guide for Care and Use of Laboratory Mice and were approved by the University of Washington Institutional Animal Care and Use Committee.

Care and maintenance of mouse lines

Mice were kept in standard mouse cages on a 12-hr light dark cycle with ad libitum water and food. Experimental mice were generated by crossing *Scn1a* heterozygous mice to homozygous *Fos2a*/homozygous tdTomato (stock # 007914, The Jackson Laboratory) mice were maintained on a C57BL/6J background (The Jackson Laboratory). *Fos2a*/tdTtomato mice were group-housed and maintained by backcrossing homozygous *Fos2a*/tdTomato mice to C57BL/6J WT mice to yield Fos2a heterozygous/ tdTomato heterozygous mice, which were bred to other, non-littermate,

heterozygous mice to yield *Fos2a/tdTomato* homozygous mice. These homozygous mice were then bred with *Scn1a* heterozygous mice to yield experimental mice. Individual litters were assigned to time points ranging from P16 to P21 and all mice from each litter were injected with the drug. Mice chosen to undergo thermal inductions were injected with the drug at P23-P24 and allowed to rest for 4-6 hours before undergoing the paradigm. Imaging studies contained both male and female mice, as no difference was observed between the two groups; therefore, the data were pooled. Mice were genotyped utilizing previously published primers (Yu et al., 2006).

4-Hydroxytamoxifen injections

Mice were injected with a 50 mg/kg dose of 4-hydroxytamoxifen (Sigma T176) dissolved in corn oil (Sigma C8267). 4-hydroxytamoxifen was chosen due to its shorter window of activity (12 hrs) than tamoxifen (24 hrs.) 4-hydroxytamoxifen was prepared by dissolving 50 mg of 4-hydroxytamoxifen in 50 ml of 100% ethanol to form stock solution of 5 mg/ml, which was stored for up to a month at -20^{o}C. Immediately before use, an equivalent amount of corn oil was added to the drug solution and the mixture was vacuum-centrifuged to remove all ethanol before it was injected into the experimental animals. After injection, animals were left to age for two weeks to allow the tdTomato reporter to express before perfusion and tissue preparation.

Thermal induction of seizures

Thermal inductions were performed as described previously (Kalume et al., 2013b). Seizures were induced at P23-P24, approximately 4-6 hours following an injection with 4-hydroxytamoxifen. Briefly, mouse body temperature was measured continuously with a rectal thermometer probe connected to a feedback temperature recorder and a heat lamp (TCAT2DF; Physitemp). Mouse body temperature was held at 36.5^{o}C for 10 min to habituate the mouse to the chamber. Following

the habituation step, the internal temperature was elevated 0.5º every two min until either the mouse had a seizure or the internal body temperature reached 41.0 ºC. If the mouse experienced any behavioral seizure activity, the severity was assessed according to the Racine Scale system (Racine et al., 1972): 1, mouth and facial movements; 2, head nodding; 3, forelimb clonus, usually one limb; 4, forelimb clonus with rearing; and 5, generalized tonic-clonic seizure (GTC), rearing, clonus, and falling over. Due to the difficulty of assessing seizures with a severity below 3, we limited our assessment to Racine 3-5 seizures. If the mouse experienced a behavioral seizure, the trial was ended. Mice were allowed to age for two weeks following thermal induction to allow for tdTomato reporter expression before perfusion and tissue extraction.

Tissue preparation and imaging

To collect tissue, mice were anesthetized with isoflurane (Piramal Enterprises LTD, NDC 66794-017-25), intracardially perfused with 4% paraformaldehyde (wt/vol) in 0.1 M Phosphate Buffer (PB) solution and allowed to post-fix for 1 h before being placed in a 15% sucrose solution in 0.1 M PB overnight. Subsequently, brains were allowed to sink for approximately 24 h in 30% sucrose in 0.1 M PB before being sectioned into 50 μm slices. Slices were mounted on coated slides and gain and offset matched images of tdTomato expressing cells were collected on a Leica Inverted Widefield microscope at the Keck Imaging Facility of the University of Washington. Individual tdTomato positive cells were counted in described brain regions using the spot-counter functionality on Imaris Image Analysis Software (Oxford Instruments) at the Keck Imaging Facility. Data files were analyzed by Imaris under the same parameters for all experimental conditions and genotypes.

Statistics

All data are expressed as the mean ± SEM or median where noted. For curve comparison, the Log-rank (Mantel-Cox) test was used to determine difference between the two conditions as indicated in the figure legends. If data met the assumptions of normally distributed data as determined by Shapiro-Wilk normality test and F test for equal variances, unpaired t-tests were used for *post hoc* analysis. For data that failed the assumptions necessary for parametric statistical techniques, we used Mann-Whitney U tests where appropriate. For all cases, statistical tests were two-tailed and the threshold of significance was set at $P < 0.05$. For figures, *$P < 0.05$; **$P < 0.01$; ***$P < 0.001$, ****$P < 0.0001$.

2.8 Figures

Fig. 1 Injection of 4-hydroxytamoxifen induces robust tdTomato reporter expression

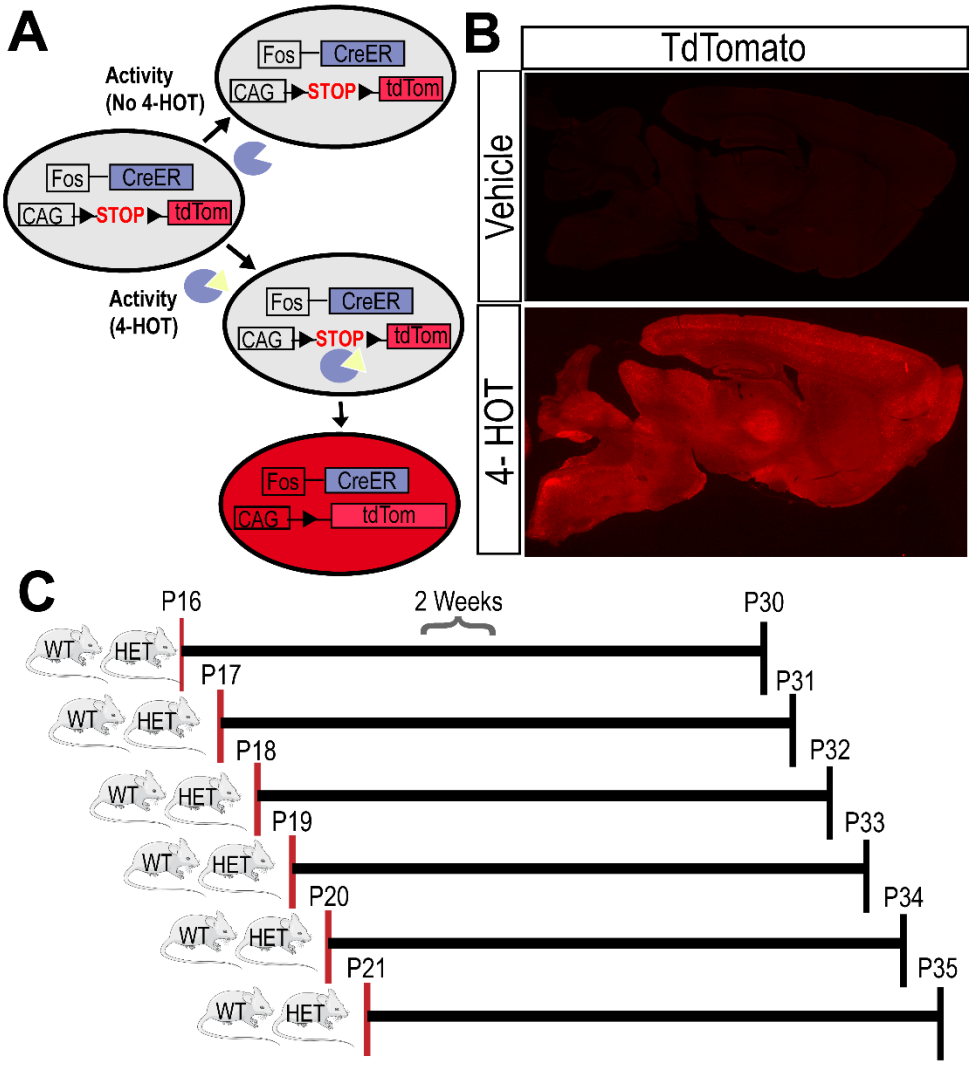

Schematic and timeline of 4-hydroxytamoxifen injections. (A) Schematic of tdTomato reporter expression following presence or absence of 4-hydroxytamoxifen. 4-HOT: 4-hydroxytamoxifen, CAG: CAG promoter, *Fos*: *Fos* promoter, CreER (B) Injection of vehicle only does not induce reporter expression, while global activation of reporter is observed upon intraperitoneal injection of 4-hydroxytamoxifen. (C) Schematic of injection cohorts of *Fos2a* WT or *Fos2a Scn1a*$^{+/-}$ (HET) mice. Red line denotes day of injection.

Fig. 2 Fos2a Scn1a$^{+/-}$ and Fos2a WT mice do not display loci of hyperactivity

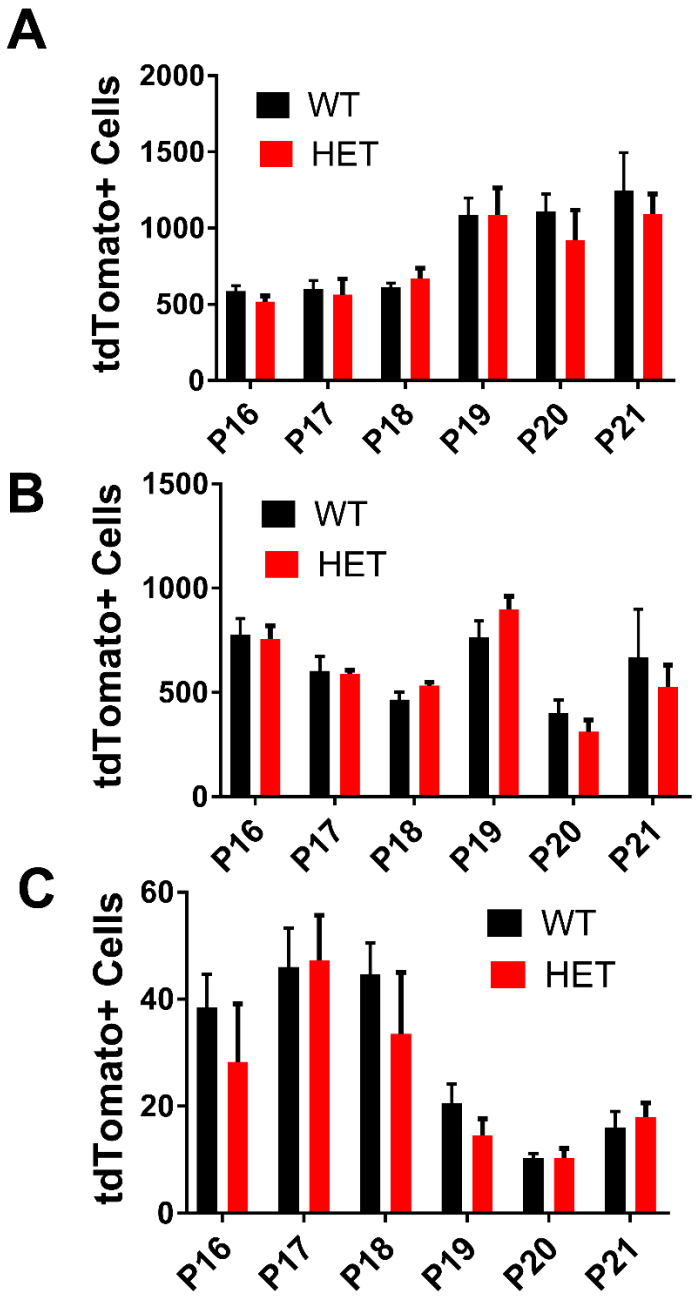

Separate cohorts of *Fos2a* WT and *Fos2a Scn1a*$^{+/-}$ mice were injected on time points ranging from P16-P21. (A) TdTomato+ cells from P16-P21 located within the visual cortex (B) TdTomato+ cells P16-P21 located within the somatosensory cortex (C) TdTomato+ P16-P21 cells located within the thalamus. WT = *Fos2a* WT; HET= *Fos2a Scn1a*$^{+/-}$

Fig. 3 Scn1a$^{+/-}$ mice do not display hyperactivity in the dorsal-medial or ventral-lateral hippocampus

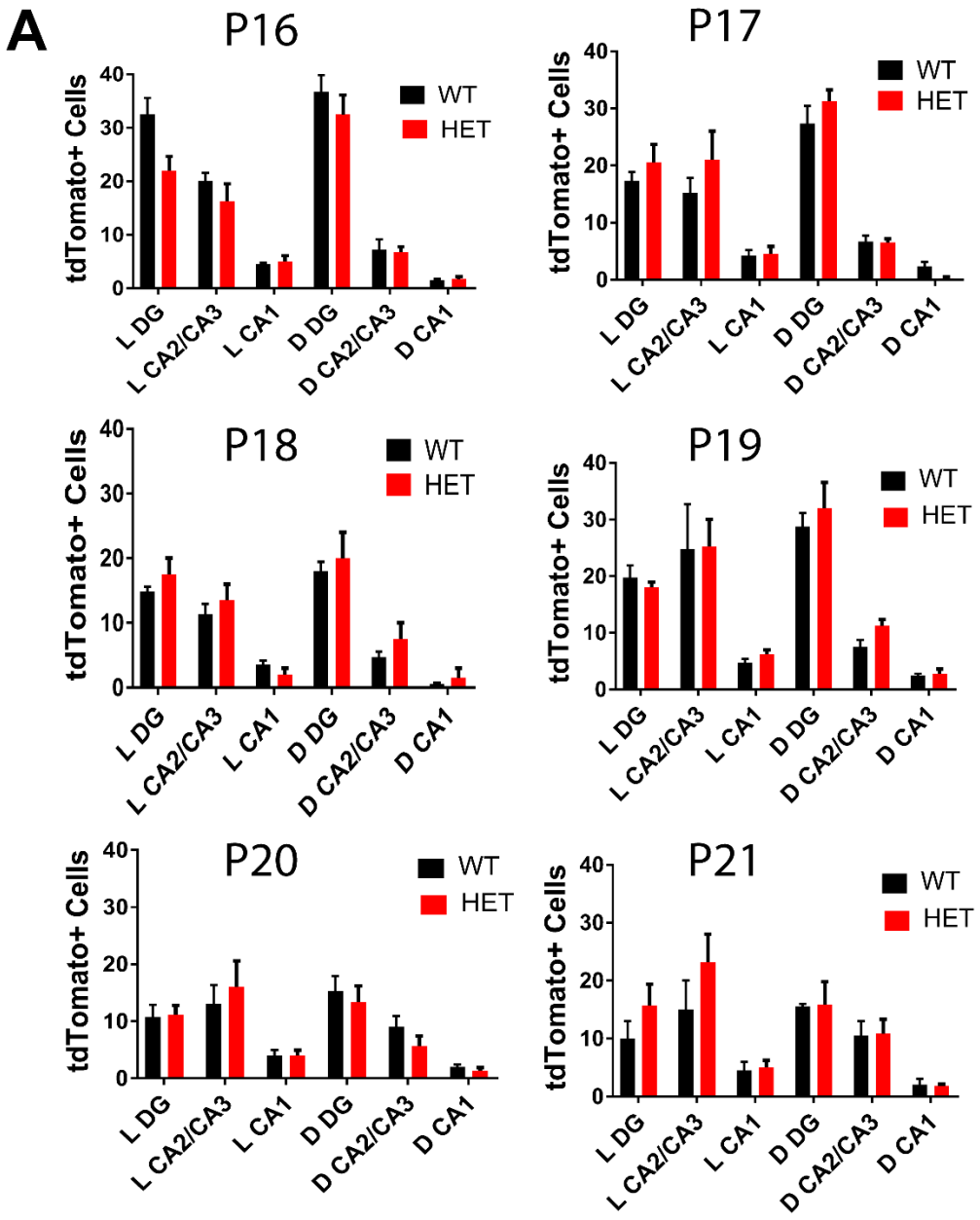

Separate cohorts of *Fos2a* WT and *Fos2a Scn1a*$^{+/-}$ mice were injected on time points ranging from P16-P21. (A) TdTomato+ cells from P16-P21 mice located within the hippocampus. L DG: Ventral-Lateral Dentate Gyrus; L CA2/CA3: Ventral-Lateral CA2/CA3; L CA1: Ventral-Lateral CA1; D DG: Dorsal-Medial Dentate Gyrus; D CA2/CA3: Dorsal-Medial CA2/CA3; D CA1: Dorsal-Medial CA1. WT = *Fos2a* WT; HET= *Fos2a Scn1a*$^{+/-}$

Fig. 4. Seizure activity upregulates cortical activity across the Fos2a Scn1a$^{+/-}$ brain

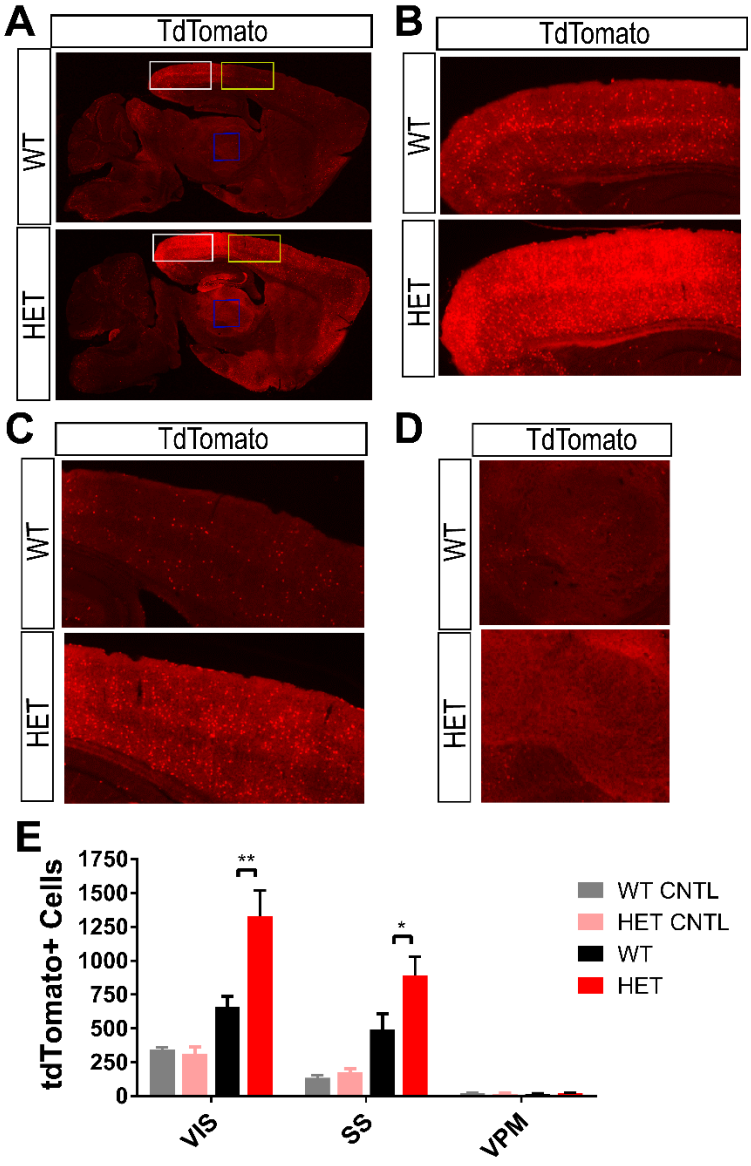

Visual Cortex (VIS), Somatosensory Cortex (SS), and thalamic (VPM) activity of *Fos2a WT* (WT) and *Fos2a Scn1a*$^{+/-}$ (HET) mice after thermal induction. A) Representitve image of WT and HET brain slices. White box = Visual Cortex; Yellow box = Somatosensory Cortex; Blue box = Ventral posteromedial nucleus of the thalamus . B) Expanded view of visual cortex between WT and HET animals C) Expanded view of somatosensory cortex (D) Expanded view of the ventral posteromedial nucleus (E) Number of TdTomato+ cells in WT and HET mice after being induced (WT and HET), or during a control paradigm (WT CNTL and HET CNTL).

Fig. 5: Epileptic activity specifically activates hippocampal dentate granule cells and CA3/CA2 pyramidal cells in Fos2a Scn1a$^{+/-}$ mice

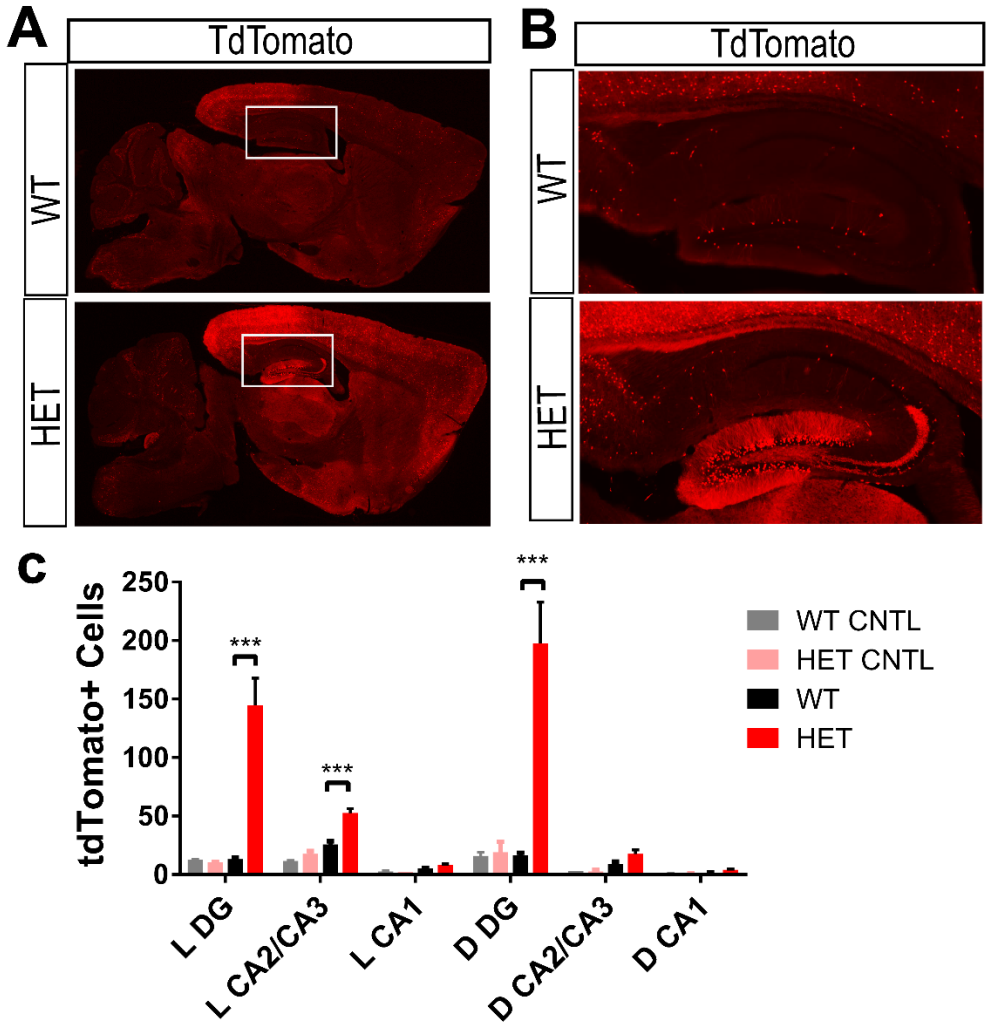

Hippocampal activity of *Fos2a WT* (WT) and *Fos2a Scn1a*$^{+/-}$ (HET) mice after thermal induction. A) Representitve image of WT and HET brain slices. Hippocampus is bounded by a white box. B) Close up of hippocampus contained C) Number of TdTomato+ cells in WT and HET mice after being induced (WT and HET), or during a control paradigm (WT CNTL and HET CNTL). DG: Ventral-Lateral Dentate Gyrus; L CA2/CA3: Ventral-Lateral CA2/CA3; L CA1: Ventral-Lateral CA1; D DG: Dorsal-Medial Dentate Gyrus; D CA2/CA3: Dorsal-Medial CA2/CA3; D CA1: Dorsal-Medial CA1. WT = *Fos2a* WT; HET= *Fos2a Scn1a*$^{+/-}$

Chapter 3: Hippocampal deletion of $Na_V1.1$ channels in mice causes thermal seizures and cognitive deficit characteristic of Dravet Syndrome

3.1 Abstract

Dravet Syndrome is a severe childhood epileptic disorder caused by haploinsufficiency of the *Scn1a* gene encoding brain voltage-gated sodium channel $Na_V1.1$. Symptoms include treatment-refractory epilepsy, cognitive impairment, autistic-like behavior, and premature death. The specific loci of $Na_V1.1$ function in the brain that underlie these global deficits remain unknown. Here we specifically deleted *Scn1a* in the hippocampus using the Cre-Lox method in weanling mice. Local gene deletion caused selective reduction of inhibitory neurotransmission measured in dentate granule cells. Mice with local $Na_V1.1$ reduction had thermally-evoked seizures and spatial learning deficits, but they did not have abnormalities of locomotor activity or social interaction. Our results show that local gene deletion in the hippocampus can induce two of the most severe dysfunctions of Dravet Syndrome: epilepsy and cognitive deficit. Considering these results, the hippocampus may be a potential target for future gene therapy for Dravet Syndrome.

3.2 Keywords

Epilepsy, *Scn1a*, Dravet, Sodium Channels, $Na_V1.1$, Spatial Learning

3.3 Significance Statement

Dravet Syndrome is an intractable epileptic disorder that includes cognitive and social-interaction deficits. It is caused by loss-of-function mutations in the brain sodium channel $Na_V1.1$. We asked whether symptoms of Dravet Syndrome could be induced by introducing the mutation only in the hippocampus, a brain region important for learning and memory and for control of brain

excitability. Local mutation of $Na_V1.1$ specifically reduced the excitability of inhibitory neurons in the hippocampus. This local mutation caused thermally evoked seizures and spatial learning deficits, which are brain-wide effects. Our results point to a key role for the hippocampus in generating epilepsy and cognitive deficit in Dravet Syndrome and suggest that gene therapy targeting the hippocampus might be effective in this devastating disease.

3.4 Introduction

Dravet Syndrome, also known as Severe Myoclonic Epilepsy of Infancy (SMEI), usually presents before the age of one year in children (Dravet, 2011a, b). Febrile seizures are the first manifestation of the disease, and they quickly evolve to spontaneous seizures that become intractable and pharmacoresistant (Dravet, 2011a, b). Multiple comorbidities accompany the disease, including cognitive and social impairments, hyperactivity, and circadian rhythm and sleep defects (Dravet, 2011a, b). The genetic etiology has been largely elucidated, with >80% of patients displaying haploinsufficiency due to a loss-of-function mutation in the *SCN1A* gene encoding the pore-forming α subunit of the brain voltage-gated sodium channel $Na_V1.1$ (Claes et al., 2003; Claes et al., 2001; Marini et al., 2009; Marini et al., 2011).

In mice, *Scn1a* heterozygotes ($Scn1a^{+/-}$) in the C57BL/6 genetic background are an accurate genocopy and phenocopy of the human disease (Catterall, 2018; Catterall et al., 2010a; Ogiwara et al., 2007; Yu et al., 2006). They have thermally induced and spontaneous seizures, hyperactivity, cognitive and social impairments, ataxia, circadian rhythm and sleep deficits, and increased risk of SUDEP (Catterall, 2018; Catterall et al., 2010a; Han et al., 2012a; Han et al., 2012b; Ito et al., 2013b; Kalume et al., 2015; Kalume et al., 2013a; Kalume et al., 2007; Oakley et al., 2009; Ogiwara et al., 2007; Yu et al., 2006). Although the global mutation is not cell-specific, reduced sodium current has been observed in GABAergic inhibitory neurons in the hippocampus, cerebral

cortex, thalamus, and cerebellum, with little or no effect on sodium current in excitatory neurons in C57BL/6 mice (Kalume et al., 2015; Kalume et al., 2007; Tai et al., 2014; Yu et al., 2006). Consistent with a major role of inhibitory neurons in this disease, heterozygous deletion of $Na_V1.1$ in forebrain interneurons recapitulates the epilepsy, premature death, cognitive and social deficits, and sleep impairment of Dravet Syndrome (Cheah et al., 2012; Han et al., 2012a; Kalume et al., 2015), and deletions in subsets of interneurons induce specific aspects of these disease phenotypes (Catterall, 2018; Rubinstein et al., 2015a; Tatsukawa et al., 2018a). In contrast, deletion of *Scn1a* in excitatory neurons does not induce disease phenotypes and actually ameliorates the severity of the disease (Ogiwara et al., 2013).

Although the major symptoms of Dravet Syndrome, including epilepsy, cognitive impairment, and social interaction deficit, are global 'whole-brain' phenotypes, it is unknown whether these global phenotypes can be induced by local deletion of the $Na_V1.1$ channel. To address this question, we focused on the hippocampus because the largest deficits in interneuron excitability are observed in the hippocampus in mice with global knockout of $Na_V1.1$ (Catterall et al., 2010a; Tai et al., 2014; Yu et al., 2006), and we found a large increase in hyperexcitability in the hippocampus during thermally induced seizures in the experiments of Chapter 1. We used viral expression methods to reduce $Na_V1.1$ channels only in the hippocampus, and we determined whether this local gene deletion can induce the global phenotypes of Dravet Syndrome.

3.5 Results

Adeno associated virus-Cre injection reduces $Na_V1.1$ expression in hippocampal neurons

To selectively reduce $Na_V1.1$ expression in the hippocampus, we utilized the *Scn1a*$^{lox/lox}$ mouse line, in which exon 25 of the *Scn1a* gene is flanked by two lox-P sites (Fig. 1*A* and *B*). Previous studies using this *Scn1a*$^{lox/lox}$ (*Scn1a* Floxed) mouse line demonstrated that introduction of Cre

recombinase (Cre) results in excision of exon 25 and subsequent elimination of *Scn1a* mRNA and $Na_V1.1$ protein as tested by PCR and immunocytochemistry with specific antibodies against $Na_V1.1$ (Cheah et al., 2012). Delivery of an adeno-associated virus (AAV) encoding Cre-recombinase into the hippocampus of these mice should result in localized $Na_V1.1$ deletion. We targeted both the dorsal medial and lateral hippocampus of postnatal day 21 mice using a virally expressed active AAV-Cre-GFP construct or an inactive AAV-ΔCre-GFP control (Fig. 1*A* and *B*). We verified that expression of GFP was present in the hippocampus and largely restricted to that structure (Fig. 1*C*). To assess the activity of Cre, we injected AAV-Cre or AAV-ΔCre into age-matched tdTomato reporter mice (Jax Stock #007914) at P21. We observed reporter signal in the AAV-Cre-injected mice but not in AAV-ΔCre mice at P42, indicating that AAV-Cre was functional *in vivo*, whereas AAV-ΔCre was not (Fig. 2). We measured $Na_V1.1$ protein by immunocytochemistry with specific antibodies (Cheah et al., 2013; Cheah et al., 2012). $Na_V1.1$ antibodies immunostained the cell bodies of neurons in the hippocampus as expected (Fig. 1*D*). Upon quantifying the mean signal intensity of each virally infected cell in AAV-Cre-injected and AAV-ΔCre-injected *Scn1a* floxed mice, we observed a significant reduction of immunocytochemical staining intensity in AAV-Cre-infected neurons vs. controls (AAV-ΔCre: Mean = 47.2 ± 1, n = 305; AAV-Cre: 13.9± 0.9, n=208; P= <0.0001) (Fig. 1*E*). These results indicate that $Na_V1.1$ protein was reduced on average by 70.6% in AAV-Cre-expressing neurons compared to control AAV-ΔCre-expressing neurons.

Scn1a deletion reduces frequency of sIPSCs recorded in dentate granule cells.

In hippocampal slices, global deletion of $Na_V1.1$ reduces the frequency of spontaneous, action potential-driven IPSCs recorded in excitatory neurons, but does not reduce the frequency of spontaneous EPSCs recorded in the same neurons (Han et al., 2012a; Kaplan et al., 2017). To test

whether AAV-Cre mediated knockdown of $Na_V1.1$ similarly caused a selective reduction in the excitability of inhibitory interneurons, we compared frequencies of spontaneous action potential-driven inhibitory postsynaptic currents (sIPSCs; E_{Cl} = 0 mV, V_h = -60 mV) and spontaneous excitatory postsynaptic currents (sEPSCs; E_{Cl} = -60 mV, V_h = -60 mV) using whole-cell voltage clamp techniques in hippocampal dentate granule cells (DGCs) in acutely prepared brain slices at P42 from mice injected with AAV-ΔCre and AAV-Cre at P21. We recorded sIPSCs in the presence of ionotropic glutamate receptor antagonists, 6-cyano-7-nitroquinoxaline-2,3-dione (CNQX; 20 μM) and 2-amino-5-phosphonovaleric acid (APV; 50 μM), to isolate IPSCs from GABAergic interneurons. DGCs from AAV-Cre mice had a strikingly reduced sIPSC frequency (2.15 ± 0.31 Hz, n = 16) compared to DGCs from AAV-Δ-Cre mice (3.79 ± 0.64 Hz, n = 10; t(24) = 2.57 , P = 0.02; Fig. 3*A* and *B*). As a control, we tested whether excitatory neurons similarly showed reduced excitability from AAV-Cre injection by measuring the frequency of sEPSCs in DGCs in the presence of the broad-spectrum $GABA_A$ receptor antagonist, GABAzine (10 μM), to isolate glutamatergic neurotransmission. In the absence of functional GABAergic inhibitory neurotransmission, sEPSC frequency was similar between DGCs from AAV-Cre (0.91 ± 0.16 Hz, n = 8) and AAV-ΔCre mice (0.98 ± 0.12 Hz, n = 11; t(17) = 0.36, P = 0.73; Fig. 3*B* and *C*). These results support the conclusion that the reduction in sIPSCs is a specific effect of AAV-Cre-mediated knockdown of $Na_V1.1$ in inhibitory neurons rather than a nonspecific effect on all synaptic transmission onto DCGs.

To further test the specificity of the reduction in IPSC frequency caused by AAV-Cre injection, we calculated the effects of GABAzine on the percent change in sEPSCs. If GABAergic inhibitory neurotransmission is specifically reduced in AAV-Cre-expressing mice, the effect of GABAzine on their excitatory neurotransmission should be correspondingly reduced compared to AAV-ΔCre-

expressing mice. Consistent with that conclusion, there was a larger GABAzine-induced increase in sEPSC frequency in AAV-ΔCre-expressing mice (85.1 ± 15.9%) than AAV-Cre-expressing mice (24.5 ± 5.79%; $t(15) = 3.40$, $P < 0.01$; Fig. 3*C* and *D*), further indicating that under control conditions, DGCs in AAV-Cre mice have a weaker inhibitory brake on glutamatergic transmission than DGCs in AAV-ΔCre mice.

Reduction of $Na_V1.1$ in the hippocampus induces thermally evoked seizures.

Febrile seizures are characteristic of early stages of Dravet Syndrome (Dravet, 2011b). To model febrile seizures in mice, we utilized a thermal induction protocol in AAV-Cre-injected and AAV-ΔCre-injected *Scn1a* floxed mice at P42, three weeks after viral injection (Oakley et al., 2009). After a habituation period, the mice were subjected to a gradual 0.5°C increase in body temperature every two min from 36.5°C to 41.0°C, which mimics the increase of body temperature during a fever. During this period, the mice were observed for behavioral epileptic activity, as quantified on the Racine scale of 1-5 (Racine et al., 1972). During this thermal induction paradigm, almost half (44%) of the AAV-Cre injected mice displayed Racine 4 and 5 seizures at an average temperature of 40.3 ± 0.2 °C, while all AAV-ΔCre-injected mice remained seizure free [AAV-Cre: n = 16; AAV-ΔCre: n: 17; P =0.0020] (Fig. 4*A* and *B*). This average temperature of seizure onset is higher than observed for global $Scn1a^{+/-}$ mice, which have seizures at a mean temperature of 38.5 ± 0.2°C (Oakley et al., 2009). Visually, we did not observe any spontaneous seizures during handling or behavior, and AAV-Cre injected mice did not die prematurely, which indicates that they do not have severe spontaneous generalized tonic-clonic seizures that induce SUDEP. These differences are most likely caused by the localized nature of the deletion in the virally injected mice. We assessed and verified viral expression in the hippocampus in each mouse, and we noticed no apparent correlation between areas of viral spread and seizure susceptibility. To verify that

these observed behavioral seizures were indeed the result of abnormal electrical activity, we implanted AAV-Cre-injected and AAV-ΔCre-injected mice with EEG leads in the left and right cerebral cortex at P35 and subjected these mice to the thermal induction protocol at P42 (Fig. 4*C*). While recordings from AAV-ΔCre mice showed no epileptiform activity (Fig. 4*D*), recordings from AAV-Cre mice displayed interictal spikes, indicative of abnormal electrical activity, during the thermal induction process (Fig. 4*E*). In AAV-Cre injected animals, thermally induced behavioral seizures were correlated with electrographic seizure activity (Fig. 4*F*). Therefore, local deletion of $Na_V1.1$ in the hippocampus is sufficient to cause interictal epileptiform discharges and thermal induction of seizures, as assessed from measurements of both abnormal behavioral and abnormal electrographic seizure activity. Additionally, we performed a series of injections only in dorsal-medial (Fig. 5*A*) or ventral lateral hippocampus (Fig. 5*B*), instead of both areas combined, and noticed no behavioral epileptic phenotypes, suggesting that a "critical mass" of $Na_V1.1$ reduction needs to occur in order to trigger thermally induced epileptic phenotypes (Fig. 5C-*D*).

Reduction of $Na_V1.1$ in the hippocampus causes a specific defect in spatial learning and memory.

Global *Scn1a* deletion results in several co-morbidities, including hyperactivity, social interaction deficit, and cognitive impairment (Han et al., 2012a; Ito et al., 2013b; Ogiwara et al., 2007). To explore the effects of targeted $Na_V1.1$ reduction in the hippocampus on mouse behavior, we used behavioral assays for locomotion, social interaction, and spatial learning. Locomotor activity was tested in the open field. We found no difference between AAV-Cre-injected mice and AAV-ΔCre-injected mice in total distance traveled, as a measure of hyperactivity, or in the amount of time spent in center of the field, as a measure of anxiety (Fig. 6*A* and *B*).

To assay the effect of hippocampal *Scn1a* deletion on social behaviors, we subjected the mice to behavioral paradigms that quantify the preference and quality of their interactions with a stranger

mouse. In the Three Chamber Test of social interaction, AAV-Cre and AAV-ΔCre mice similarly demonstrated a significant preference for social interaction by spending more time in close proximity to the cage containing a stranger mouse compared to an identical empty cage, as measured by an interaction ratio ($P < 0.0001$ for both groups) (Fig. 7*A*-*C*). To examine social interactions in a less confined setting, we used the reciprocal interaction paradigm, which assesses the behavior of mice placed in an open field as they freely interact with a stranger mouse. AAV-Cre mice engaged in a similar number of nose-to-nose interactions, nose-to-anogenital interactions, and rapid escape behaviors as their AAV-ΔCre littermates (Fig. 7*D*). These results indicate that *Scn1a* deletion in the hippocampus is not sufficient to induce impaired social interaction behaviors.

Cognitive abilities are often measured with tests of learning and memory. Novel object recognition memory refers to the ability of a mouse to judge a previously encountered object as familiar vs. a new object as novel. This test is considered a measure of cerebral cortical function when the spatial position of the objects is not part of the test cue (Winters et al., 2004). Mice with global deletion of *Scn1a* do not display defects in novel object recognition (Han et al., 2012a). Similarly, both AAV-Cre and AAV-ΔCre mice significantly preferred interacting with a novel object over a familiar object during the novel object recognition paradigm, as measured by an interaction ratio ($P < 0.0001$ for both groups) (Fig. 8*A*-*C*).

As global *Scn1a* deletion results in severe impairments in spatial learning and memory (Han et al., 2012a; Rubinstein et al., 2015a), we wondered whether these deficits would also be caused by a local genetic perturbation. We first tested the effects of hippocampal AAV-Cre injection on spatial learning, a task that requires hippocampal function (Eichenbaum et al., 1990; Morris et al., 1982; Vann and Albasser, 2011). To assess spatial learning in the absence of other stimuli, we used the

Barnes circular maze (Barnes, 1979). Both AAV-Cre and AAV-ΔCre mice were trained three times per day for four consecutive days to find a target hole containing a dark escape box located on the edge of a brightly illuminated circular platform. Over the course of training, AAV-Cre mice demonstrated impaired learning, as they required significantly longer to find the escape hole compared to their AAV-ΔCre littermates on trials 8-12 ($P < 0.043$ for trials 8-12) (Fig. 9*A*). During the probe trial on the test day following completion of the 12 training trials, AAV-Cre mice spent less time near the escape hole (AAV-ΔCre Median: 14.3, n=15; AAV-Cre Median 3.05, n=16; $P <0.0001$) (Fig. 9*B-D*), took longer to approach the escape hole (AAV-ΔCre Median: 4.57, n=15; AAV-Cre Median: 54.9, n=16; $P = 0.0055$) (Fig. 9*E*), and exhibited fewer nose pokes into the escape hole (AAV-ΔCre Median: 16, n=15; AAV-Cre Median: 3.5, n=16; $P = <0.0001$) (Fig. 9*F*). Thus, deletion of *Scn1a* in the hippocampus recapitulated one of the spatial learning deficits seen in global mouse models of Dravet Syndrome.

Spatial learning is often tested in the context of a fearful situation, because fear enhances learning and memory. We measured fear-related spatial learning with the context-dependent fear-conditioning test (Crawley, 1999), in which mice associate spatial context with a fear-inducing mild foot shock. Global *Scn1a*$^{+/-}$ mice have a major deficit in this test of fear-related spatial learning. Surprisingly, neither the AAV-Cre nor AAV-ΔCre mice demonstrated defects during context-dependent fear-conditioning. All mice displayed robust freezing behavior after being placed back into a fearful spatial context 30 min, 24 h, and 7 d after a training session in which a mild foot shock was administered in an easily recognizable spatial context (Fig. 10). Therefore, learning and memory deficits in AAV-Cre are specific to spatial learning and memory and can be overcome under more intense fear-induced learning conditions in which the salience of the spatial

cues is increased. Similarly, when *Scn1a* was deleted in a smaller subset of the hippocampus (dorsal medial only), the animals did not display any behavioral deficits (Fig. 11*A-D).*

3.6 Discussion

Global disease phenotypes from local gene deletion.

Neurogenetic diseases are caused by mutations that are expressed throughout the brain and nervous system. There are few prior examples of diseases in which local genetic changes are found to induce neurologic syndromes that can impact the activity of the entire brain. Previous studies of Dravet Syndrome fit this pattern, in that gene deletion in the entire mouse brain or in subsets of inhibitory neurons throughout the mouse brain cause specific, global disease phenotypes (Cheah et al., 2012; Kalume et al., 2015; Kalume et al., 2013a; Rubinstein et al., 2015a; Tatsukawa et al., 2018a). Here we take this analysis of Dravet Syndrome pathophysiology to a deeper level by showing that local reduction of $Na_V1.1$ channels in the hippocampus is sufficient to induce brain-wide phenotypes including generalized epilepsy and impaired spatial learning and memory. These global phenotypes may evolve as a consequence of changes in cerebral cortex functionality induced by impaired control of hippocampal excitability. Therefore, these diverse brain-wide phenotypes of Dravet Syndrome may be generated by local changes in neuronal excitability that induce broad effects on electrical activity and cognitive function in the brain.

Inhibitory neurons in Dravet Syndrome.

Like the mutations that cause Dravet Syndrome, our AAV-Cre-mediated gene deletion does not discriminate between excitatory and inhibitory neurons. However, previous work supports the conclusion that effects on inhibitory neurons are primary (Catterall, 2018). Heterozygous deletion of $Na_V1.1$ consistently causes reduced excitability of GABAergic inhibitory interneurons in

C57BL/6 mice that have the most severe Dravet Syndrome phenotypes (Han et al., 2012a; Ogiwara et al., 2013; Rubinstein et al., 2015a; Rubinstein et al., 2015b; Tai et al., 2014; Yu et al., 2006). Deletion only in inhibitory interneurons causes Dravet Syndrome phenotypes (Cheah et al., 2012; Han et al., 2012a; Kalume et al., 2015; Kalume et al., 2013a). Deletion in excitatory neurons does not induce Dravet Syndrome, and it actually ameliorates some disease phenotypes (Ogiwara et al., 2013). However, in mice with mixed genetic backgrounds and milder Dravet Syndrome phenotypes, increased excitability of excitatory neurons is also observed later in neuronal development, and one study showed that observed deficits in parvalbumin-positive fast-spiking interneurons in the barrel cortex disappeared by P35 (Favero et al., 2018; Mistry et al., 2014). These secondary effects of gene deletion may contribute to early development of seizure frequency and intensity in Dravet Syndrome and later amelioration of those phenotypes in adulthood in mice with heterozygous genetic background having a mild Dravet Syndrome phenotype (Mistry et al., 2014). Nevertheless, it is likely that the global disease phenotypes we have observed here are caused by gene deletion in the inhibitory interneurons in the hippocampus. Consistent with this, we observed a selective reduction in GABAergic, but not glutamatergic signaling to the DGCs when $Na_V1.1$ channels are reduced in the hippocampus. Therefore, we think it is likely that local deletion in inhibitory neurons is responsible for the strong epileptic and cognitive effects we have observed in our mouse model in C57BL/6 mice.

Our studies further support the importance of the hippocampus in seizure initiation and propagation and in spatial learning and memory. Repetitive stimulation of the hippocampus can kindle sustained epilepsy (Lothman et al., 1992). Surgical resection of the hippocampus impairs spatial learning and memory (Morris et al., 1982). Manipulation of the excitability of the dentate gyrus results in epilepsy in previously healthy mice (Krook-Magnuson et al., 2015; Krook-

Magnuson et al., 2014). Hippocampal interneurons have the largest loss of sodium current in Dravet Syndrome mice (Catterall et al., 2010a; Han et al., 2012a; Hedrich et al., 2014; Ogiwara et al., 2007; Yu et al., 2006). Together with these precedents, our results highlight the hippocampus as a key focus of Dravet Syndrome pathophysiology.

Although our results highlight the importance of the hippocampus for epilepsy and cognitive deficit in Dravet Syndrome, other brain regions also are likely to play a key role in these deficits and other co-morbidities. Excitability of interneurons in the cerebral cortex is impaired in Dravet Syndrome mice (Hedrich et al., 2014; Tai et al., 2014), and this deficit is likely to contribute to epilepsy, cognitive deficit, and autistic-like behaviors in Dravet Syndrome. Impaired electrical excitability of interneurons in the thalamus is likely to be involved in epilepsy and sleep disorder (Kalume et al., 2015). Similarly, impaired excitability of cerebellar Purkinje neurons is likely to be important in the characteristic ataxia of Dravet Syndrome (Kalume et al., 2007). Thus, the co-morbidities of Dravet Syndrome are likely to be generated in multiple regions of the brain, but the hippocampus evidently plays a key role in two of the most serious aspects of the disease: epilepsy and cognitive deficit (Stein et al., 2019).

3.7 Methods

All experiments were carried out in C57BL/6J mouse genetic background. Our methods for mouse husbandry, thermal induction of seizures, and behavioral experiments follow our previously published protocols (Han et al., 2012a; Oakley et al., 2009) and are described in detail in Methods. Experiments were performed according to guidelines established in the National Institutes of Health Guide for Care and Use of Laboratory Mice and were approved by the University of Washington Institutional Animal Care and Use Committee.

Care and maintenance of mouse lines

Mice were kept in standard mouse cages on a 12-hr light dark cycle with ad libitum water and food. Scn1a floxed mice were generated as described previously (Cheah et al., 2012), and maintained on a C57BL/6J background (The Jackson Laboratory). *Scn1a* floxed mice maintained on a C57Bl6J background are functionally wild-type and are behaviorally indistinguishable from their WT littermates. Mice were group-housed and maintained by backcrossing homozygous Scn1a floxed mice to C57BL/6J WT mice to yield *Scn1a* floxed heterozygous mice, which were bred to other, non-littermate, heterozygous floxed mice to yield Scn1a homozygous floxed mice. These homozygous *Scn1a* floxed mice were then bred with each other to yield experimental mice. Littermates of the same sex were randomly assigned to AAV-Cre or AAV-ΔCre experimental groups at P21, when the surgeries were performed. Epilepsy and electrophysiological studies contained both male and female mice, and as no difference was observed between the two groups, the data were pooled. Separate cohorts of mice were used for the behavioral experiments, which contained only male mice to maintain consistency with previously published behavioral *Scn1a*$^{+/-}$ data (1, 2). tdTomato reporter mice (stock # 007914) were purchased from The Jackson Laboratory and group housed. Floxed *Scn1a* mice were genotyped using the primers FHY311 (5′-CTTGATGTGTTGAAATTCAC-3′) and FHY314 (5′-TATAGAGTGTTTAATCTCAAC-3′): WT allele, 846 bp; floxed allele, 1019 bp; and excised allele, 258 bp.

Immunohistochemistry

Immunohistochemical procedures were performed as described previously with slight modifications (Cheah et al., 2012). Mice were anesthetized with isoflurane (Piramal Enterprises LTD, NDC 66794-017-25), intracardially perfused with 4% paraformaldehyde (wt/vol) in 0.1 M Phosphate Buffer (PB) solution and allowed to post-fix for 1 h before being placed in a 15%

sucrose solution in 0.1 M PB overnight. Subsequently, brains were allowed to sink for approximately 24 h in 30% sucrose in 0.1 M PB before being sectioned into 50 μm slices and labeled as free-floating sections. Briefly, tissue was rinsed in 0.1 M Tris buffer (TB) and 0.1 M Tris buffered saline (TBS), blocked with an Avidin/Biotin blocking kit (Vector Biolabs, SP-2001), and incubated with rabbit anti-$Na_V1.1$ primary antibody (1:175, Millipore AB 5204A). Subsequently, the tissue was incubated in biotinylated goat anti-rabbit IgG (Vector Biolabs, BA-1000), followed by incubation in a secondary antibody, which was a goat anti-rabbit IgG labeled with Streptavidin, Alexa Fluor™ 555 Conjugate (1:1000; Thermo Fisher, S32355). Tissue samples from AAV-Cre and AAV-ΔCre mice were processed simultaneously. Gain and offset matched images of GFP expressing cells were collected on a Leica SP8X confocal microscope at the Keck Imaging Facility of the University of Washington. Sections stained without primary antibody showed no detectable labeling. For all experiments, we verified that GFP reporter expression was present in the hippocampus; any mice with no expression or inappropriate expression were eliminated. To verify the activity of expressed AAV-Cre recombinase, we performed immunohistochemical staining and subsequent analysis using Imaris Image Analysis Software (Oxford Instruments) of AAV-Cre and AAV-ΔCre injected tissue labeled with the $Na_V1.1$ antibody (1:175, Millipore AB 5204A). Individual GFP positive cells (infected by virus) were analyzed for mean NaV1.1 intensity through the entire volumetric cell using the Imaris Image Analysis Software (Oxford Instruments). Data files were analyzed by Imaris under the same parameters for both experimental conditions.

Thermal induction and analysis of seizures

Thermal inductions were performed as described previously (Kalume et al., 2013b). Seizures were induced at P42 via a thermal induction protocol, three weeks after injection of the virus or three

weeks after injection of the virus and one week after EEG implantation. Briefly, mouse body temperature was measured continuously with a rectal thermometer probe connected to a feedback temperature recorder and a heat lamp (TCAT2DF; Physitemp). Mouse body temperature was held at 36.5°C for 10 min to habituate the mouse to the chamber. Following the habituation step, the internal temperature was elevated 0.5° every two min until either the mouse had a seizure or the internal body temperature reached 41.0 °. If the mouse experienced any behavioral seizure activity, the severity was assessed according to the Racine Scale system (Racine et al., 1972): 1, mouth and facial movements; 2, head nodding; 3, forelimb clonus, usually one limb; 4, forelimb clonus with rearing; and 5, generalized tonic-clonic seizure (GTC), rearing, clonus, and falling over. Due to the difficulty of assessing seizures with a severity below 3, we limited our assessment to Racine 3-5 seizures. If the mouse experienced a behavioral seizure, the trial was ended.

Viral production and infection

Cre and ΔCre expressing pAAV1-CBA GFP DNA plasmids were kindly provided by Dr. Larry Zwiefel. Briefly, recombination deficient AAV vectors were grown with AAV1 coat serotype in human embryonic kidney (HEK293T cells). The virus was then purified with sucrose and CsCl gradient centrifugation steps, and finally resuspended in 1x HBSS at a functional titer of 1×10^6 (Gore et al., 2013). Prior to injection, viral aliquots were stored at -80°C.

P21 *Scn1a* floxed littermates were randomly assigned to AAV-Cre or AAV-ΔCre groups. Injections were performed at P21, which is the day that they are old enough to be weaned. This eliminated the need to reintroduce the pups to their dam, which can often result in overgrooming and damage to the surgical site. Mice were given a subcutaneous injection of Ketoprofen (5 mg/kg, Sigma-Aldrich, K2012) 30-60 min before the surgery to control for post-operative pain, a procedure that was repeated up to every 24 h for 48 h. The mice were anesthetized with inhaled

isoflurane (Piramal Enterprises LTD, NDC 66794-017-25) and placed in a stereotaxic device (Kopf Instruments, Model 962). The hair was shaved above the skull and bupivacaine (1 mg/kg, AuroMedics Pharma LLC, 167-10) and lidocaine (1 mg/kg, Fresenius Kabi USA, 491257) were injected underneath the skin as a local anesthetic. The skin was cut over the midline, and using a coordinate system (Paxinos and Franklin), holes were drilled in the appropriate locations (Doral Medial: -1.9 AP, ±1.5 ML, -1.8 DV; Ventral Lateral: -3.3 AP, ±2.52 ML, -4,-3,-2 DV). Either AAV-Cre or AAV-ΔCre was injected at a rate of 125 nl/min, and the needle was allowed to sit for 3 min before being withdrawn to prevent backflow. Note that virus injected at these coordinates does not cover the entire hippocampus.

Electrophysiology

Slices were placed in a submersion chamber on an upright microscope and viewed with an Olympus 40× (0.9 N.A.; BX51WI) water-immersion objective with differential interference contrast and infrared optics and were perfused with oxygenated aCSF (2 mL/min). DGCs were distinguished by their location, appearance, and physiological properties. Positive viral expression was assessed by GFP expression. Recordings were only made if positive GFP expression in the dentate gyrus was confirmed. Whole-cell recordings were made using patch pipettes constructed from thick-walled borosilicate glass capillaries and filled with internal solutions optimized for current- or voltage-clamp recordings of sIPSCs or sEPSCs, as described below. Filled patch pipettes had resistances ranging between 3 and 5 MΩ. The internal solution for all current-clamp experiments was as follows (in mM): 132.3 K-gluconate, 7.7 KCl, 4 NaCl, 0.5 $CaCl_2$, 10 Hepes, 5 EGTA free acid, 4 ATP Mg^{2+} salt, 0.5 GTP Na^+ salt, pH buffered to 7.2–7.3 with KOH. The internal solution for measuring sIPSCs (V_h = −60 mV; ECl = 0 mV) in voltage clamp was as follows (in mM): 130 CsCl, 4 NaCl, 0.5 $CaCl_2$, 10 Hepes, 5 EGTA, 4 ATP Mg^{2+} salt, 0.5 GTP Na^+

salt, 5 QX-314, pH buffered to 7.2–7.3 with CsOH. sIPSCs were measured in the presence of ionotropic glutamate receptor antagonists, CNQX (20 μM) and APV (50 μM). The internal solution for measuring sEPSCs (Vh = −60 mV; ECl = −60 mV) in voltage clamp was as follows (in mM): 145 Cs-Gluconate, 2 $MgCl_2$, 10 Hepes, 0.5 EGTA, 2 ATP-Tris, 0.2 GTP Na^+ salt, pH buffered to 7.2–7.3 with CsOH. Recordings were obtained through a multiclamp 700A amplifier (Molecular Devices) by pCLAMP 8.0 software (Molecular Devices). Drugs were dissolved in aCSF and bath-applied for a minimum of 7 min before analysis. Data from electrophysiology experiments were analyzed using Clampfit 9.0 (Molecular Devices) software. Access resistance was continuously monitored for each cell. Cells were discarded if access resistance changed by >15%. Only one cell was recorded from each brain slice if slices were exposed to pharmacological agents.

EEG surgeries and recordings

Surgeries to implant EEG electrodes were performed at P35, two weeks after the mice had undergone viral injection surgery. This allowed the mice time to recover after the initial surgeries. Both male and female mice were used, and no difference was noticed between the two groups. Mice were given a subcutaneous injection of Ketoprofen (5 mg/kg, Sigma-Aldrich, K2012) 30-60 min before the surgery to control for post-operative pain, a procedure that was repeated up to every 24 h for 2 days. The mice were anesthetized with inhaled isoflurane (Piramal Enterprises LTD, NDC 66794-017-25) and placed in a stereotaxic device (Kopf Instruments, Model 962). The hair was shaved above the skull and bupivacaine (1 mg/kg, AuroMedics Pharma LLC, 167-10) and lidocaine (1 mg/kg, Fresenius Kabi USA, 491257) were injected underneath the skin as a local anesthetic. The skin was cut over the midline, and four silver electrodes were anchored into the skull. Two recording electrodes were placed bilaterally in the cortex, and a third reference

electrode was placed into the cerebellum (Fig. 3*C*). A grounding electrode was placed near the left anterolateral edge of the frontal bone. Mice were allowed to recover from the surgery for one week and EEG recordings were acquired in conscious mice using a 3-Channel EEG tethered mouse system (Pinnacle Technology Inc, 8200-SE3 Mouse System) during the thermal induction protocol. In order to correlate seizure activity to EEG activity, mice were simultaneously videotaped for review (WinAVI Video Capture; ZJMedia Digital Technology).

Behavioral tests

For our behavioral tests, each mouse went through multiple, non-invasive procedures with a minimum of 48 h between each behavioral task to allow the mice to rest. Behavioral procedures were recorded with an HD ceiling mounted camera, and performed as described previously with slight modifications (Han et al., 2012a). Each data file was analyzed by Ethovision XT 14 (Noldus Technologies) according to the same parameters. For every mouse, the final behavioral test was the contextual fear conditioning, which requires an aversive stimulus. This test was performed last to avoid stressing the mice and confounding the other behavioral tests. Cohorts of male *Scn1a* floxed littermates were randomly assigned to experimental groups and injected at P21 with AAV-Cre or AAV-ΔCre. Behavioral experiments started at P80-90 and lasted to approximately P110. Mice were group-housed for most of this period and were separated to be singly housed and handled for 5 days before testing began. Only male mice were used for behavioral experiments to maintain consistency with previously published behavioral *Scn1a*$^{+/-}$ data (Cheah et al., 2012; Han et al., 2012a).

Open field

Mice were placed in the lower left corner of a 40 cm X 40 cm arena and allowed to freely explore for 10 min. Their movement was recorded by a HD ceiling mounted camera. Total distanced

traveled was measured, as well as the amount of time the mouse spent in the center of the arena, which comprised a circle having 25% of the area in the center of the chamber. Each data file was analyzed by Ethovision XT 14 (Noldus Technologies) according to the same parameters. The enclosure was wiped with paper towels and 70% ethanol between every subject.

Reciprocal interaction

A stranger mouse (identified by a black mark on its tail) and experimental mouse were simultaneously placed into a 40 cm X 40 cm arena. The experimental mouse was allowed to freely interact with the sex matched stranger mouse for 10 min. Their movement was recorded by a ceiling mounted camera. The enclosure was wiped with paper towels and 70% ethanol in between each subject. The recorded video file was analyzed off-line by R.S, who was blinded to the identity of the experimental mouse until after analysis. Three distinct types of interactions were counted: nose to nose sniffing, nose to anogenital sniffing, and escape behavior, characterized by a darting movement away from the stranger mouse.

Three-chamber test of social interaction

The mice were tested for social interaction preference in a three-chambered apparatus (58 × 30 cm), which is a nontransparent plastic box with two partitions, which divide the box into three equivalently sized chambers (Left, Center, Right; each 30 × 19.3 cm). In the bottom center of each internal partition is a small square opening, which allows the mouse to freely pass into each of the three chambers. In the habituation phase, the experimental mouse was placed in the central chamber and allowed to explore the apparatus for 10 min. Following this 10-min habitation phase, the experimental mouse was removed and small cylindrical wire cages (10.5-cm diameter; Galaxy Pencil Cup; Spectrum Diversified Designs) were introduced into the top left and right corners of

the apparatus. Cylindrical bottles of water were placed on top of these wire cups to prevent the mouse from climbing on top of them. One of the cages was empty and the other contained a sex- and aged-matched stranger C57BL/6J mouse. The experimental mouse was then re-introduced and allowed to explore the chambers again for 10 min. The side of the apparatus that contained the stranger mouse was counterbalanced in between trails. The wire cages and chamber were cleaned with 70% ethanol and wiped with paper towels between each test mouse. The experimental mouse's movement was recorded by a HD ceiling mounted camera. All data were analyzed under the same parameters between trials (EthoVision XT 14.0, Noldus Technology). Time spent in each chamber and time spent in a proximal circle 5 cm from each of the wire cages was recorded.

Barnes maze

The Barnes maze apparatus is a white, opaque, circular piece of plexiglass (92 cm diameter) containing 20 equally spaced holes (7 cm diameter) located 5 cm from the perimeter. A black escape box (15 x 7 x 7 cm) is placed under one hole. The maze was set up 1 m above the floor in a room containing a multitude of contextual cues, which did not change throughout the course of the experiment. Two bright lights (200W) were used to illuminate the surface of the maze. The experimental mouse's movement was recorded by a HD ceiling mounted camera. The experimental mouse, after being allowed to habituate to the maze for 2 min on the first day, underwent 3 trials (with approximately 20 min between trials) per day for 4 days where the mouse was placed in the center of the maze and given 3 min to explore. If the mouse entered the escape hole, the trial was finished and the lights were switched off for 1 min before placing the mouse back in its home cage. If the mouse didn't find the escape hole during the 3-min trial, the trial was ended and the mouse was gently guided into the escape box and the lights were turned off. The escape box and maze were cleaned with 70% ethanol and wiped with paper towels between each

test mouse. On the test day, the escape box was removed and mouse was placed on the maze for 3 min. Parameters measured (EthoVision XT 14.0, Noldus Technology) included time the mouse spent within a proximal circle of 5 cm around the correct hole, number of times the mouse placed its head into the target hole which used to contain the escape box, and latency to the correct hole. The wire cages and chamber were cleaned with 70% ethanol and wiped with paper towels between each test mouse, and all data was analyzed under the same parameters between trials.

Context-dependent fear conditioning

The contextual fear conditioning apparatus was a square (25 x 25) arena with clear plexiglass floor and a wire grid bottom which was connected to an amplifier that could be set to deliver shocks to the metal grid bottom and controlled by software (Freeze Frame 2.0, Actimetrics). The movement of mice was recorded by a USB webcam (LifeCam HD-6000, Microsoft) and PC-based video-capture software (WinAVI Video Capture, ZJMedia Digital Technology). On Day 1, a mouse was introduced into the chamber and allowed to habituate by exploring the chamber for 2 min. After two min, the mouse received a single mild foot shock (2 s, 0.6mA) and was removed from the chamber after an additional min. Thirty min after the habituation/training session, the mouse was returned to the chamber and recorded for 2 min. This same procedure was repeated 24 h after the training session and 7 days after the training session. The arena cleaned with 70% ethanol and wiped with paper towels between each test mouse. Percent freezing was calculated offline using the recorded video by the video-tracking software (EthoVision XT 9.0, Noldus Technology). Freezing behavior was defined as the amount of time in which the velocity of the experimental mouse was below 1.75 cm/s, and all data were analyzed under the same parameters between trials.

Novel object recognition

Novel object recognition was performed in a square, opaque, plexiglass chamber (40 x 40 cm). The experimental mouse's movement was recorded by an HD ceiling mounted camera. During the habituation session, a test mouse was allowed to freely explore for 10 min. Following this habituation stage, two objects of similar size but different shape and color (Duplo Bricks) were placed in opposite corners of the arena 14 cm from the corner. The mouse was allowed to explore these objects for another 10 min. After a 2 min delay, the test mouse was placed back into the chamber, in which one of the "familiar" objects had been replaced by a novel object. The mouse was allowed to explore these objects for another 10 min. To avoid odor cues, a duplicate of the familiar object was used. The arena and objects were cleaned with 70% ethanol and wiped with paper towels between each test mouse. Time spent within a 5 cm proximal circle centered on each object was measured using Ethovision XT 14 (Noldus Technology), and all data was analyzed under the same parameters between trials. The arena cleaned with 70% ethanol and wiped with paper towels between each test mouse.

Statistics

All data are expressed as the mean ± SEM or median where noted. For curve comparison, the Log-rank (Mantel-Cox) test was used to determine difference between the two conditions as indicated in the figure legends. If data met the assumptions of normally distributed data as determined by Shapiro-Wilk normality test and F test for equal variances, unpaired t tests were used for *post hoc* analysis. For data that failed the assumptions necessary for parametric statistical techniques, we used Mann-Whitney U tests where appropriate. For all cases, statistical tests were two-tailed and the threshold of significance was set at $P < 0.05$. For figures, *$P < 0.05$; **$P < 0.01$; ***$P < 0.001$, ****$P < 0.0001$.

3.9 Figures

Fig. 1. AAV-Cre injection reduces $Na_V1.1$ expression in hippocampal neurons.

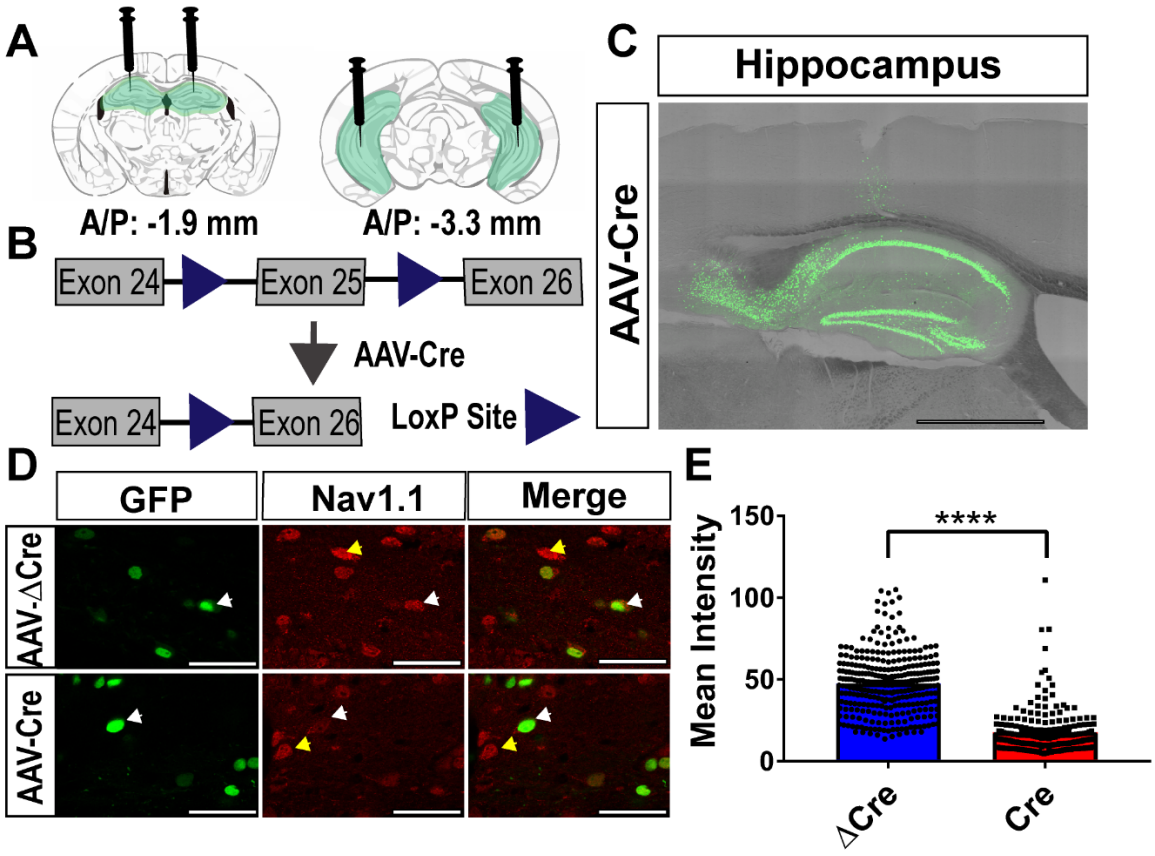

AAV-ΔCre and AAV-Cre viruses were injected into the hippocampus of P21 *Scn1a* floxed mice, and tissue was harvested three weeks later at P42 (*A*) Schematic showing placement of the injection sites (Dorsal Medial: -1.9 AP, ±1.5 ML, -1.8 DV; Ventral Lateral: -3.3 AP, ±2.52 ML, -4,-3,-2 DV) in coronal slices of the mouse brain. Green = GFP expression from viral infection. (*B*) Exon 25 of the *Scn1a* gene is excised upon introduction of the AAV-Cre virus. Triangles = loxP sites. (*C*) Representative image of viral infection in a sagittal slice of hippocampus. AAV-Cre = viral infection, Scale bar = 500 µm. (*D*) Representative images of $Na_V1.1$ expression in AAV-Cre and AAV-ΔCre infected cells in the hilus of the hippocampus. White arrows indicate $Na_V1.1$ expressing virally infected neurons. Yellow arrows indicate $Na_V1.1$ expressing neurons that are not infected with virus. Scale bar = 50 µm. (*E*) Quantification of mean intensity of GFP+ infected hippocampal neurons. Mann-Whitney rank sum test: AAV-ΔCre: Median = 47.2, n = 305; AAV-Cre: 13.9, n=208; P= <0.0001.

Fig. 2. AAV-Cre expressing virus activates reporter expression.

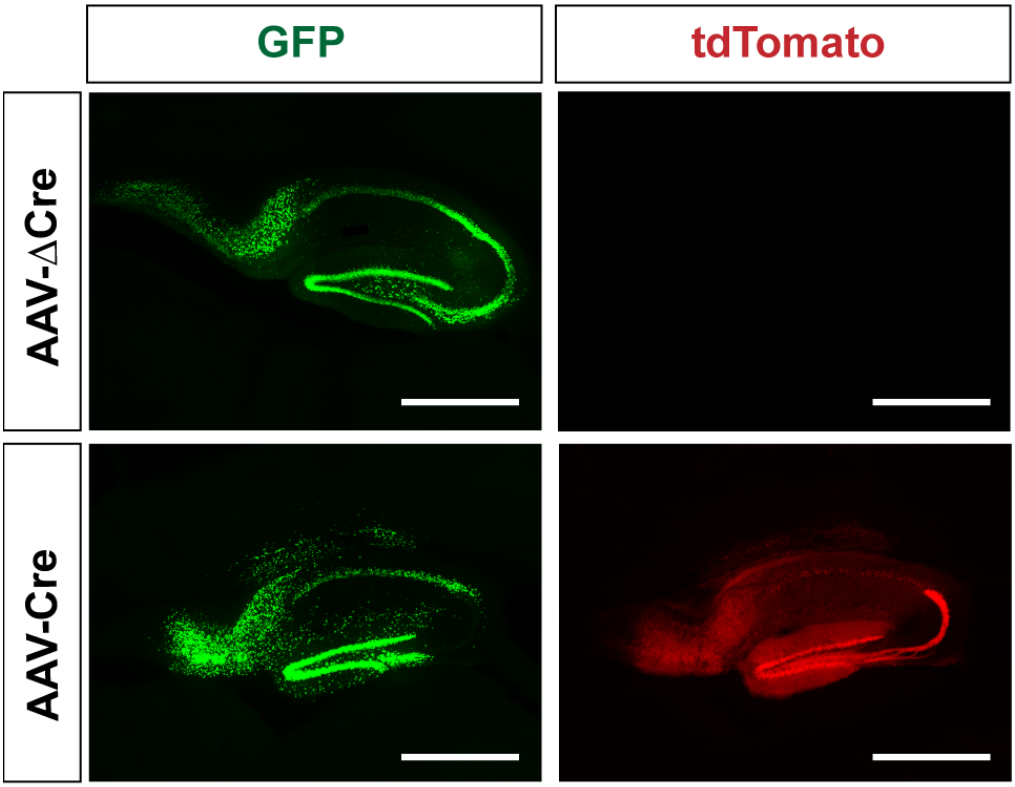

AAV-ΔCre and AAV-Cre injection in the hippocampus (GFP, green) and tdTomato reporter expression (tdTomato, Red). Scale bar = 500 μm.

Fig. 3. Selective reduction in GABA$_A$ receptor-mediated transmission in AAV-Cre injected mice.

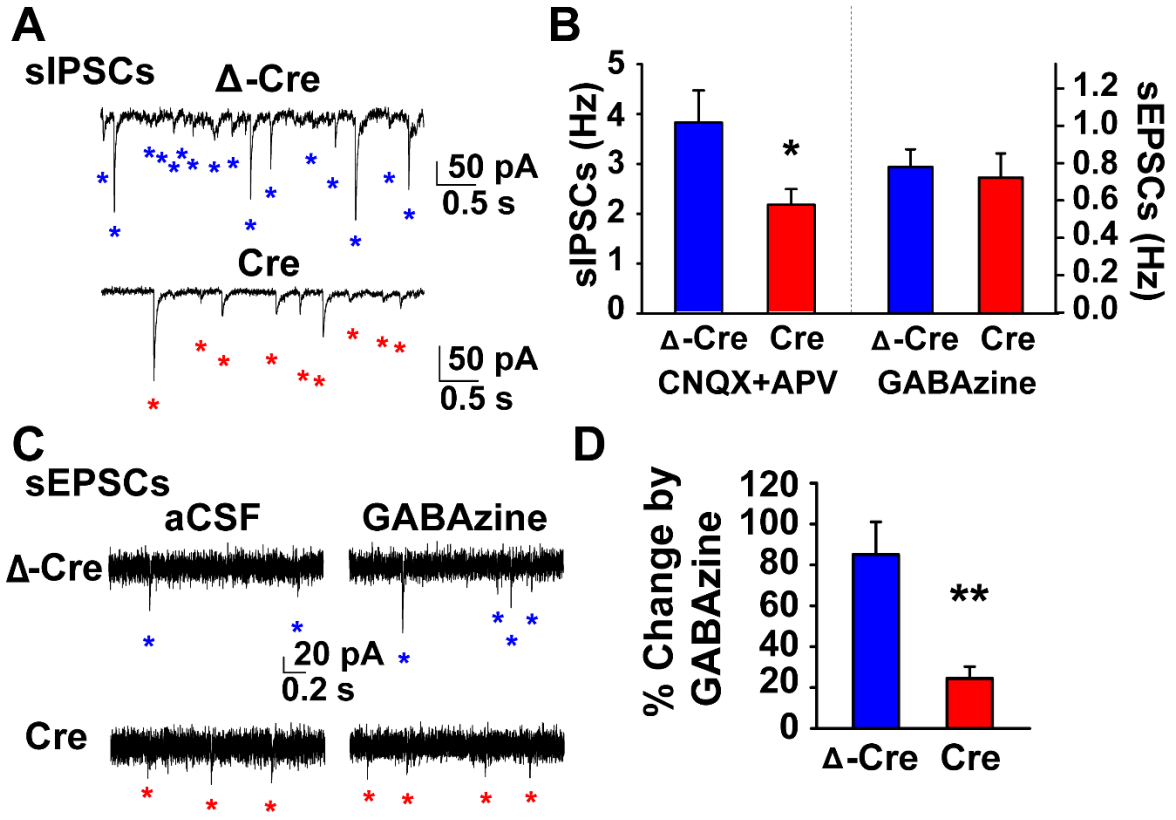

Voltage-clamp recordings were conducted at P42 on *Scn1a* floxed mice injected at P21 with either AAV ΔCre or AAV Cre (*A*) Representative voltage-clamp recordings (E_{Cl} = 0 mV; V_h = -60 mV) of DGC sIPSCs from -ΔCre (top, blue) and AAV-Cre-injected mice (bottom, red) in the presence of ionotropic glutamate receptor antagonists, CNQX (20 μM) and APV (50 μM). Individual sIPSCs are indicated with an asterisk. (*B*) Summary chart showing the mean sIPSC frequency in CNQX and APV (Unpaired two-tailed Student's t-test: left; AAV-Δ-Cre: 3.79 ± 0.64 Hz, n = 10; AAV-Cre: 2.15 ± 0.31 Hz, n = 17; t(24) = 2.57, P = .017) and sEPSC frequency in GABAzine (Unpaired two-tailed Student's - test: right; AAV-Δ-Cre: 0.98 ± 0.12 Hz, n = 11; Cre: 0.91 ± 0.16 Hz, n = 8; P = 0.73). (*C*) Representative voltage-clamp recordings (E_{Cl} = -60 mV; V_h = -60 mV) of DGC sEPSCs from AAV-Δ-Cre (top, blue) and AAV-Cre injected mice (bottom, red) in aCSF (left) and the presence of the broad spectrum GABA$_A$ receptor antagonist, GABAzine (right, 10 μM). Individual sEPSCs are indicated with an asterisk. (*D*) Summary chart showing the percent change in sEPSC frequency caused by GABAzine (Unpaired two-tailed Student's t-test: AAV-ΔCre: 85.1 ± 15.9%, n = 9; AAV-Cre: 24.5 ± 5.79, n = 8; t(15) = 3.40, P = 0.004). Data are represented as mean ± SEM.

Fig. 4. Reduction of hippocampal Na$_V$1.1 is sufficient to induce thermally evoked seizures.

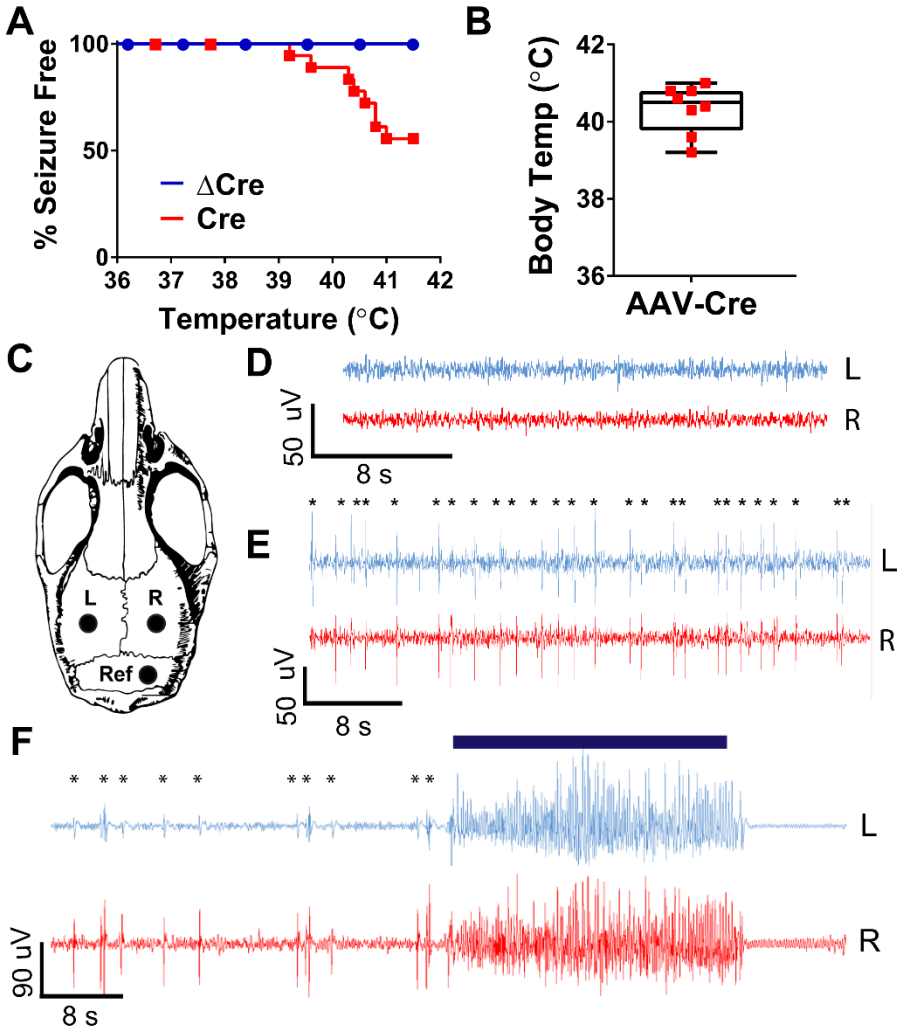

Scn1a floxed mice were injected at P21 with AAV-ΔCre or AAV-Cre virus. Mice were either allowed to age to P42 and them thermally induced to test for thermally evoked seizures, or they were implanted at P35 with EEG electrodes and then electrographically recorded during thermal induction one week later at P42. (*A*) Percent of AAV-Cre and AAV-ΔCre mice remaining seizure-free after thermal induction. (AAV-ΔCre: 100%; AAV-Cre: 66%). (*B*) Core body temperature at which AAV-Cre injected mice had seizures (AAV-Cre: 40.3 ± 0.2 ºC). (*C*) Schematic of placement of left cortical electrode [L], right cortical electrode [R], and reference electrode [Ref] during EEG implantation surgery. (*D*) Representative cortical EEG trace of an AAV-Cre-injected mouse during the habituation period before the thermal induction protocol. (*E*) AAV-Cre-injected mouse experiencing interictal events during thermal induction protocol; asterisks denote myoclonic events. (F) Myoclonic events leading up to a behavioral seizure in an AAV-Cre injected mouse; asterisks represent myoclonus, blue bar indicates observed behavioral Racine 5 seizure.

Fig. 5. Subdividing hippocampal $Na_V1.1$ deletion does not result in behavioral seizures

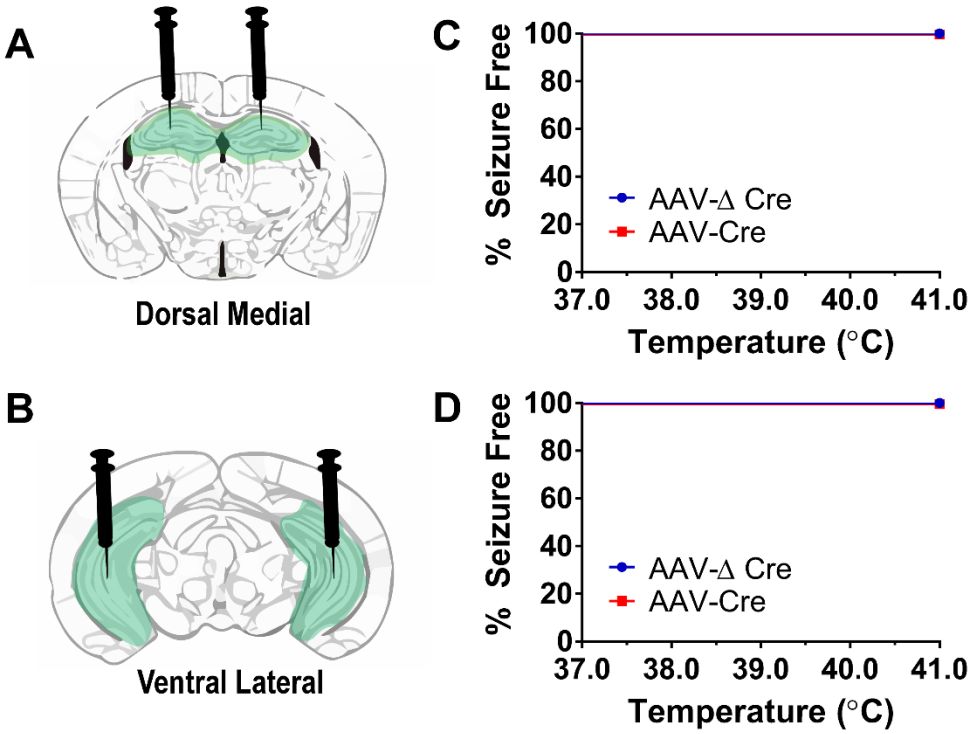

Scn1a floxed mice were injected at P21 with AAV-ΔCre or AAV-Cre virus in injections which subdivided the two original injection locations (Dorsal Medial: A/P -1.9 and Ventral lateral: A/P -3.3) into two different cohorts. Mice were either injected bilaterally at the dorsal medial location OR the ventral lateral location, allowed to age to P42, and then thermally induced to test for thermally evoked seizures. (*A*) Schematic illustrating dorsal-medial (A/P-1.9) only injection. (*B*) Schematic illustrating ventral lateral (A/P -3.3) only injection. (*C*) Percent of Dorsal Medial AAV-Cre and AAV- ΔCre mice remaining seizure free after thermal induction (AAV-ΔCre: 100%, N = 18; AAV-Cre: 100%, N = 15). (D) Percent of Ventral Lateral AAV-Cre and AAV- ΔCre mice remaining seizure free after thermal induction (AAV-ΔCre: 100%, N = 5; AAV-Cre: 100%, N = 4).

Fig. 6. Deletion of Scn1a in the hippocampus does not affect behavior in the open field.

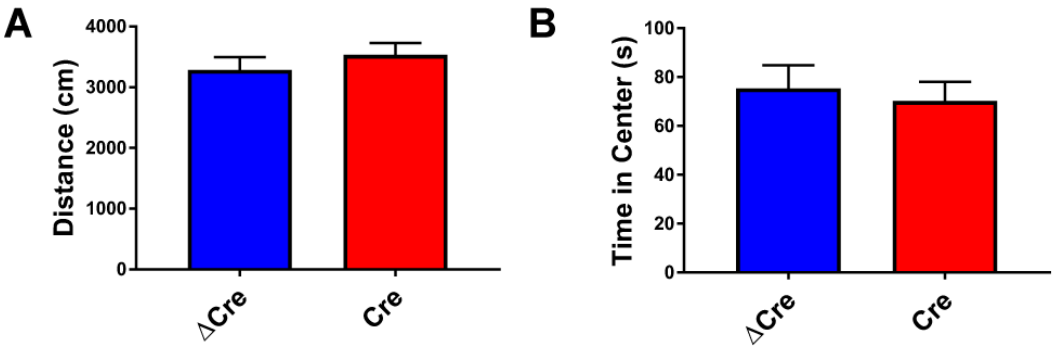

(*A*) Distance travelled during time min spent in open field chamber. Unpaired two-tailed Student's t test: Left, AAV-ΔCre: 3285 ± 211 n=16; Right, AAV-Cre: 3531 ± 194, n=17; P = 0.40. (*B*) Amount of time spent in center of open field. Unpaired two-tailed Student's t test: Left, AAV-ΔCre: 75.4 ± 9.39, n=16; Right, AAV-Cre: 70.2 ± 7.80, n=17; P = 0.67. Data are represented as mean ± SEM.

Fig. 7. Scn1a deletion in the hippocampus does not cause social interaction deficits

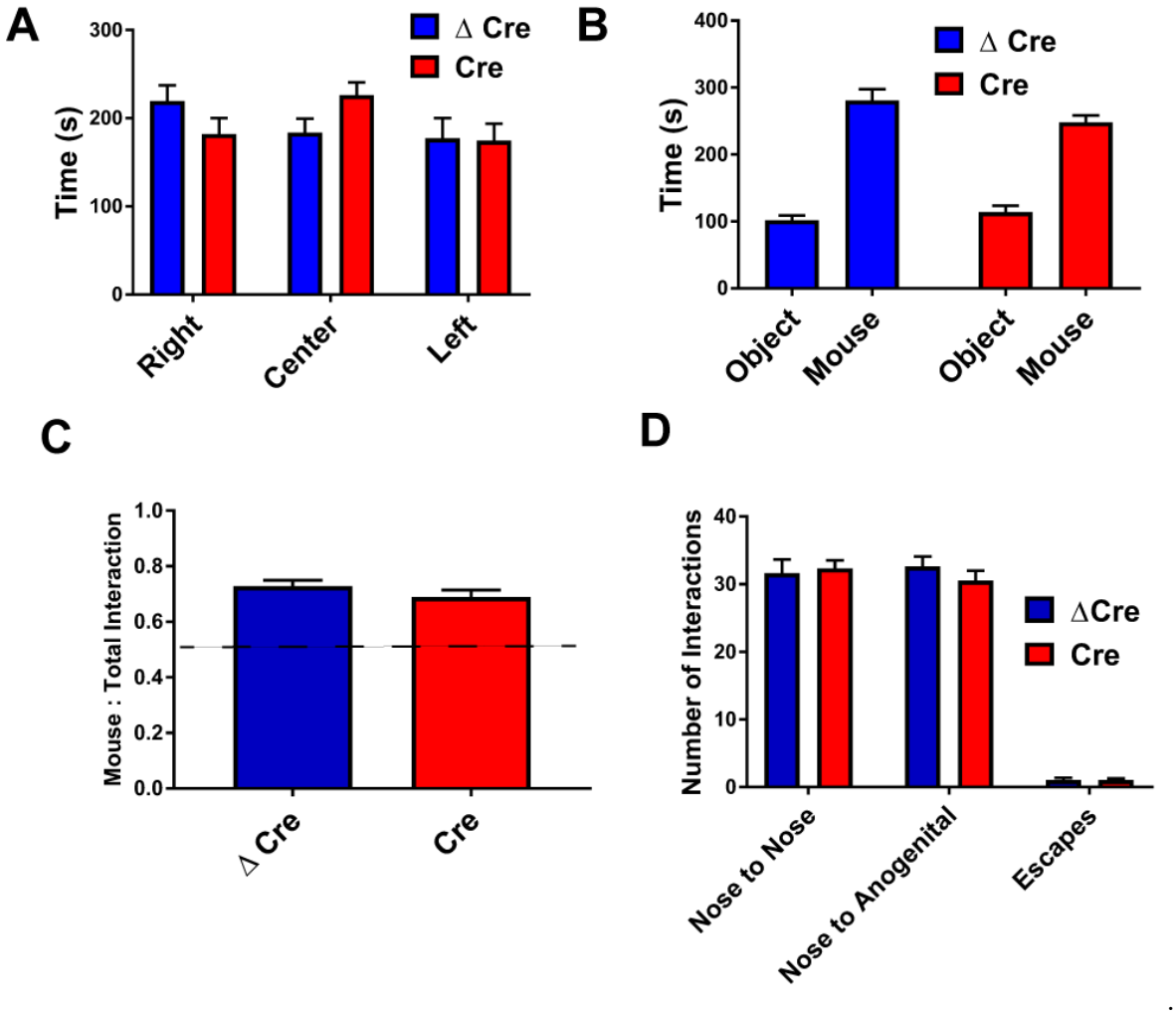

AAV-ΔCre or AAV-Cre injected *Scn1a* floxed mice were habituated for ten min in an empty 3-chambered box, removed, and re-introduced to the box following placement of two pencil cups (one empty, one containing a stranger mouse) in opposite chambers. The test mouse was then allowed to freely explore the chambers for ten min. (*A*) Habituation period for 3-chamber test of social interaction for AAV-ΔCre (blue) and AAV-Cre (red) injected mice. (*B*) Total time (s) spent with either the object (O) or mouse (M). (*C*) Ratio of time spent with mouse to total interaction time with both objects. Unpaired two-tailed Student's t-test: Left, AAV-ΔCre: 0.73 ± 0.021, n=16; Right AAV-Cre: 0.69 ± 0.026, n=15; P = 0.24. (*D*) Number of nose-to-nose, nose-to-anogenital, and escape behaviors. Data are represented as mean ± SEM.

Fig.8. Scn1a deletion in hippocampus does not cause impairments in novel object recognition.

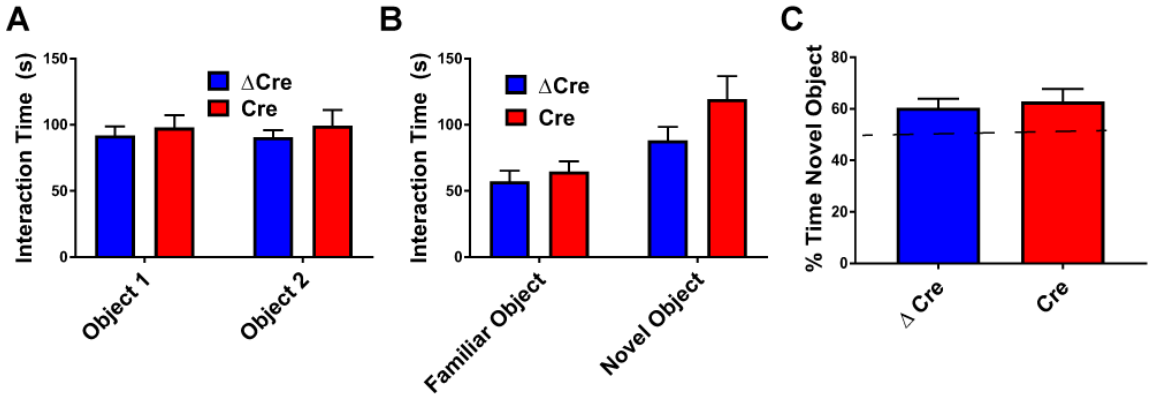

(*A*) Amount of time (s) AAV-ΔCre (Blue) and AAV-Cre (Red) spent with the familiar object. (*B*) Amount of time (s) spent with a familiar object vs. a novel object. (*C*) Ratio of time spent with novel object to total time spent interacting with both objects. Unpaired two-tailed Student's t test: AAV-Cre: 60.4 ± 3.5, n=10; AAV-ΔCre: 62.8 ± 4.9, n=9; P = 0.69. Data are represented as mean ± SEM.

Fig. 9. Scn1a deletion in the hippocampus leads to defects in spatial memory.

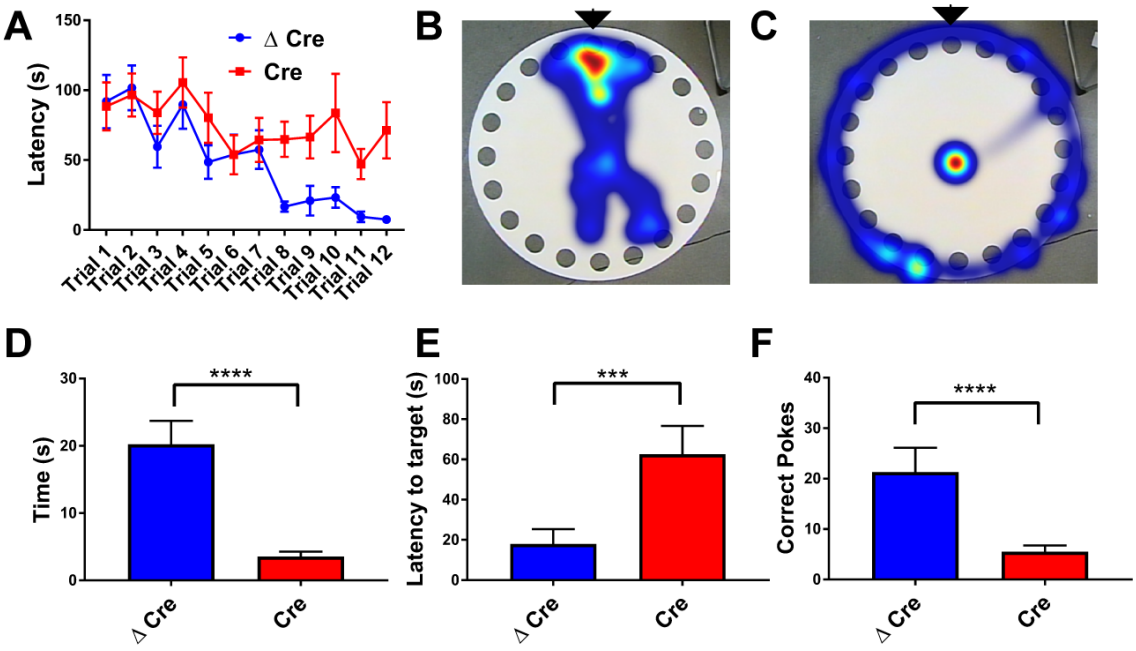

AAV-ΔCre or AAV-Cre injected *Scn1a* floxed mice were placed on a raised circular platform containing eighteen holes. One hole contained a removable escape box. Mice were trained on a series of training trials to find the escape box; when the mouse entered the escape box, the training trial was ended. On the test day, the escape box was removed. (*A*) Latency to escape box during 12 total training trials over 4 days ($P < 0.042$ for Trials 8-12). (*B*) Heat map of the location of an AAV-ΔCre injected mouse during the test day trial. Location of escape box during trial days is marked with a black arrow. (*C*) Heat map of the location of an AAV-Cre injected mouse during the test day trial. Location of escape box during trial days is marked with a black arrow. (*D*) Time spent near correct hole during the test day (Mann-Whitney rank sum test; AAV-ΔCre Median: 14.3, n=15; AAV-Cre Median 3.05, n=16; $P < 0.0001$). (*E*) Latency to target hole during the test day. Mann-Whitney rank sum test; AAV-ΔCre Median 4.57, n=15; AAV-Cre Median 54.9, n=16; $P = 0.0055$. (*F*) Number of times a mouse poked its nose into the correct hole. Mann-Whitney rank sum test; AAV-ΔCre Median: 16, n=15; AAV-Cre Median: 3.5, n=16; $P = <0.0001$.

Fig. 10. Scn1a deletion in the hippocampus does not cause impairment in context-dependent fear conditioning.

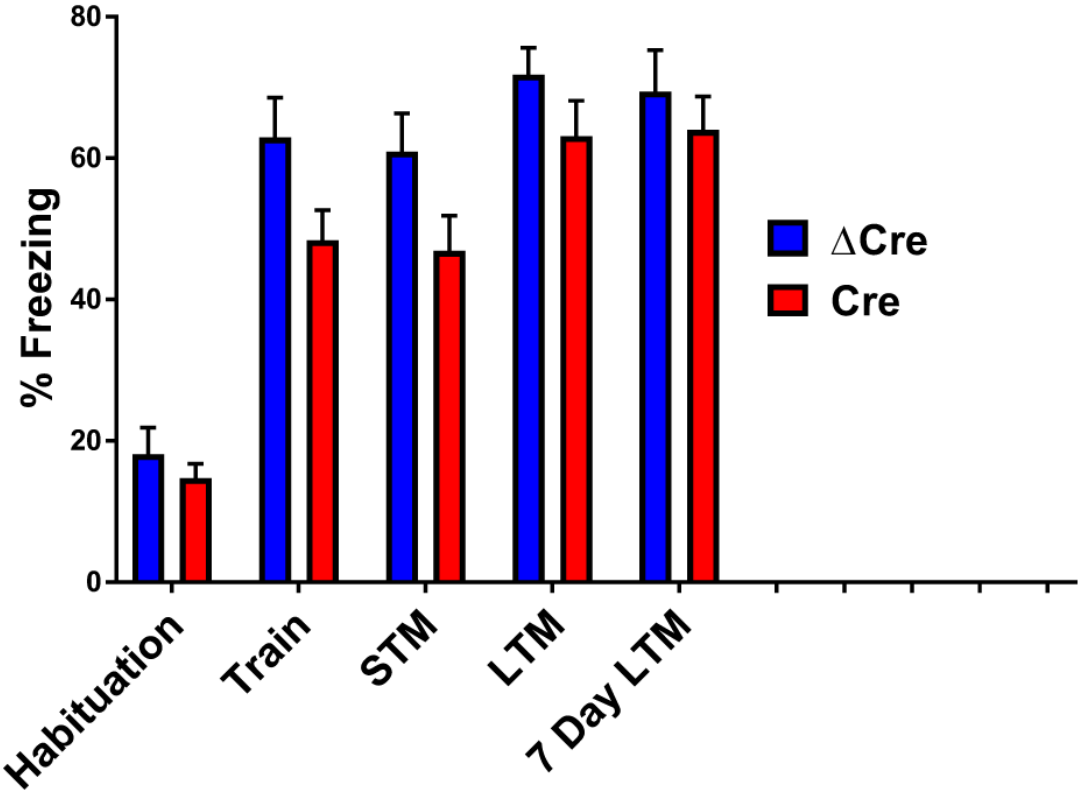

Freezing behavior was recorded in AAV- ΔCre or AAV-Cre injected *Scn1a* floxed mice during a series of two-min trials before and at designated time points after a mild foot shock. Mice were habituated for two min in a box containing a wire floor grid, after which they received a foot shock. Freezing behavior was calculated during the two-min habituation (Pre-foot shock), training (immediately after foot shock), 30-min short-term memory, 24-h long-term memory, and 7-day long-term memory trials. Blue = AAV-ΔCre, N = 15; Red = AAV-Cre, N = 16. Data are represented as mean ± SEM.

Fig. 11. Subdividing hippocampal Na$_V$1.1 deletion does not result in any measured behavioral abnormalities

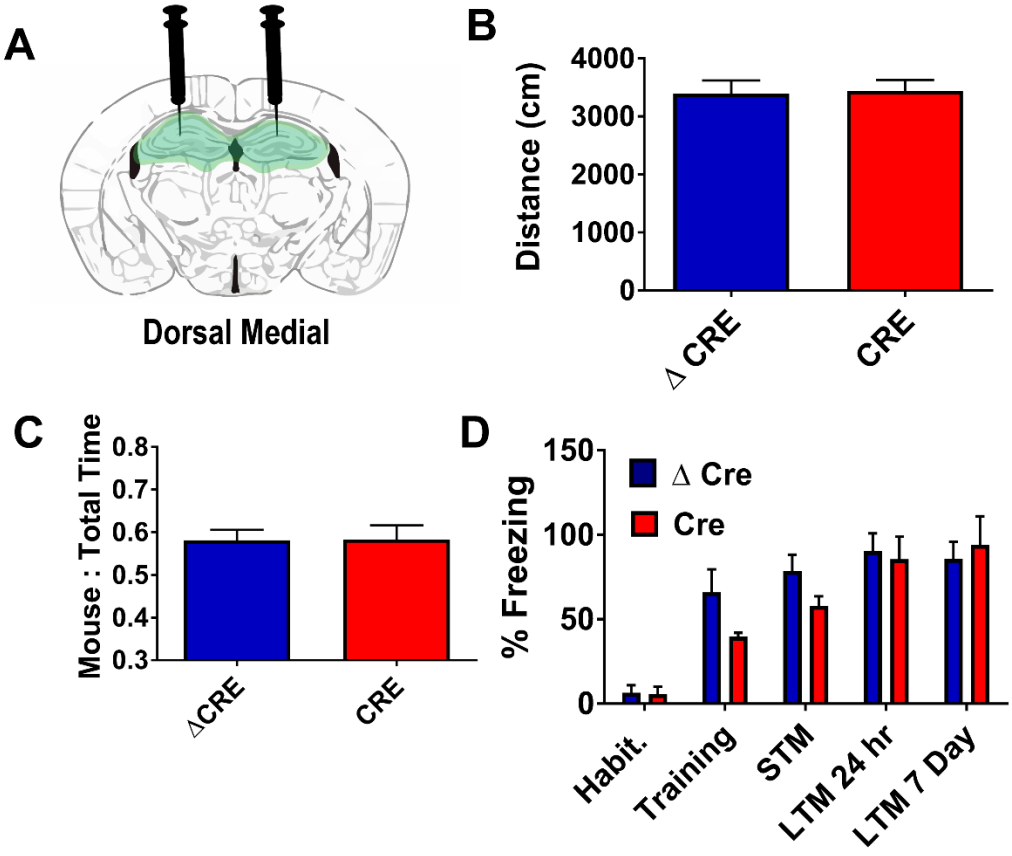

Mice were bilaterally injected at P21 with AAV only in the dorsal-medial hippocampus and put through several behavioral paradigms (*A*) Schematic illustrating dorsal-medial (A/P-1.9) only injection. (*B*) No difference in distance travelled during time min spent in open field chamber. AAV-ΔCre, N = 12; AAV-Cre, N = 11. (C) No difference in preference for interacting with a novel mouse compared to an empty pencil cup AAV-ΔCre, N = 12; AAV-Cre, N = 11. (D) Freezing behavior during a series of two-min trials before and at designated time points after a mild foot shock. Mice were habituated for two min in a box containing a wire floor grid, after which they received a foot shock. Freezing behavior was calculated during the two-min habituation (Pre-foot shock), training (immediately after foot shock), 30-min short-term memory, 24-h long-term memory, and 7-day long-term memory trials. Blue = AAV-ΔCre, N = 4; Red = AAV-Cre, N = 4. Data are represented as mean ± SEM.

Chapter 4: Future of Genetic Therapies for Dravet Syndrome

4.1 Advances in Genetic Editing

Genetic editing, enabled by the discovery of the Clustered Regularly Interspaced Short Palindromic Repeats (CRISPR)-associated endonuclease Cas9 and its variants, has enabled researchers to specifically mutate or repair sections of DNA. Guided by a single-strand guide RNA (gRNA) to a target region of DNA located near a specific protospacer-adjacent motif (PAM) site, Cas enzymes cause double stranded breaks (DSBs) in DNA. Double-stranded breaks in DNA are repaired within the cell in two distinct ways: non-homologous end joining (NHEJ) and homology directed repair (HDR). In NHEJ, proteins known as Ku heterodimers bind to the cut ends of the DNA and then serve as guides for different repair proteins. However, this process is quite error prone and indels are often introduced when the strands are misaligned or degraded, leading to mutations which can cause frameshifts and knock out an entire gene. Therefore, by introducing DSBs in targeted regions of the genome, researchers can use CRISPR to cause gene knock-outs with a high degree of penetration. In HDR, Rad51 proteins may bind these DSB cut ends, which can recruit other factors that assist with genetic recombination if homology arms are present on a strand of template DNA. Therefore, researchers can introduce genetic modifications or can repair targeted point mutations in the genome (Sander and Joung, 2014; Xiao-Jie et al., 2015). Although it was originally thought that HDR wasn't possible in post-mitotic cells such as neurons, recent studies with Adeno-Associated viruses (AAVs) have demonstrated the efficacy of HDR insertion via donor template to neuronal populations (Gaj et al., 2016).

4.2 Novel Therapeutic Approaches to Dravet Syndrome.

As a genetic disease caused by loss-of-function mutations, the ideal permanent therapeutic approach to Dravet Syndrome is to re-express the affected gene in appropriate brain regions or to use CRISPR/Cas9 methods to repair the gene defect in affected brain regions. While whole brain re-expression or gene repair might eventually be attainable, and recent papers have indeed demonstrated that broad infection with AAV is possible (Deverman et al., 2016; Massaro et al., 2018), the risk of widespread off-target effects and the desire for treatment specificity could limit this approach. Our results showing that two of the major deficits in Dravet Syndrome, epilepsy and cognitive deficit, can be generated by gene mutation specifically in the hippocampus, and that during an epileptic seizure, various regions of the hippocampus are hyperactive, opens the possibility for future application of gene re-expression or gene repair technologies in the hippocampus using surgical procedures developed for intractable temporal lobe epilepsy. Thus, our studies have important implications for understanding the molecular and cellular basis of Dravet Syndrome and for formulating new therapeutic strategies that selectively target the key brain regions contributing to its phenotypes.

4.3 CRISPR/Cas9 Repair of Point Mutations in Dravet Syndrome

Ongoing experiments in the laboratory seek to utilize the CRISPR/Cas9 methodology to repair a nonsense mutation (R1407X) which occurs near the end of exon 21 of the *Scn1a* gene in a knock-in mouse line of Dravet syndrome. This mutation reflects one found in the human population, and these mice display the core Dravet Syndrome symptoms of SUDEP, spontaneous seizures, autistic-like characteristics, ataxia, and cognitive deficits (Ito et al., 2013a; Oguni et al., 2005; Tatsukawa et al., 2018b). Due to its single point mutation and the location of the mutation close to intron 22, this mouse model represents an excellent model to test CRISPR/Cas repair as a proof of principle

in Dravet Syndrome. Therefore, we have begun the process of applying AAV-mediated CRISPR-Cas9 techniques to the R1407K model of Dravet Syndrome to examine the feasibility of restoring $Na_V1.1$ functionality in the hippocampus and its downstream effects on epileptic susceptibility and behavioral deficits.

In short, we will utilize a single AAV vector system, validated to facilitate targeting with high efficacy, to express SaCas9 and the associated guide RNA in the hippocampus of R1407X Dravet Syndrome mice. To facilitate HDR, a second AAV virus containing the single-strand donor template will be injected concurrently into the hippocampus at P21, and the mice will then be examined for seizure susceptibility and behavioral impact compared to mice injected with a nonspecific guide RNA sequence. In order to maximize success in vivo, we have first attempted to test this system *in vitro* in a cell line (Neuro-2a) chosen for ease of transfection and sequence similarity.

In vitro studies of CRISPR-cas9 repair in Neuro-2a cells

In order to avoid further loss of function in the healthy copy of *Scn1a,* we designed specific CRISPR guides (sgRNA) to target the intronic sequence proximal to Exon 21. To do so, we selected three candidate guides, which were chosen based on their proximity to the R1407 codon in Exon 21, and their low predicted off-target effects: 133fwd (195 BP away from R1407), 156RV (218 BP away from R1407), and 137RV (199 BP away from R1407). These oligos were annealed and then sub-cloned into the Px601 vector using BSaI cut sites (Ran et al., 2015) . Neuro-2a cells, derived from albino A mice, were sequenced to confirm homology of the repair and guide sites compared to the R1407X Dravet Syndrome mouse, bred on a C57Bl6J background. To verify cutting efficacy and choose the optimal gRNA, cells will be transfected with one of the three

SaCas9-U6-sgRNA and assayed using PCR techniques for detecting indel formation, signaling that a cutting event has taken place.

During future experiments, we will generate the AAV virus AAV1-CMV-SaCas9-U6-sgRNA using previously described methods as well as a second AAV1 virus containing the template strand comprising of a sequence with homology to the 500 bp upstream and downstream from the cut site. These homology arms will contain a the X1407R repair sequence as well as a mutated PAM sequence to prevent re-cutting of the repaired section of DNA (Fig. 1A-C).

In vitro studies of CRISPR-Cas9 repair in the R1407X mouse.

Following verification of targeting efficacy and repair *in-vitro,* we will co-inject the AAV1-CMV-SaCas9-U6-sgRNA virus along with a GFP reporter virus, AAV1-CMV-KASH-GFP in the hippocampus of P21 R1407X Dravet Syndrome mice. After allowing sufficient time for repair (yet to be determined), we will dissect the hippocampus, FACS sort for GFP+ cells, isolate DNA and PCR amplify to check for targeting efficacy.

Experimental and control animals will be assayed using a variety of electrophysiological and behavioral paradigms to assess excitatory/inhibitory inputs into the dentate gyrus granule cells, seizure severity, and behavioral co-morbidities.

4.5 Thesis Summary

Taken together, the results gathered in my graduate work highlight the role of the hippocampus in the symptoms of Dravet Syndrome. Induction of seizures in Dravet Syndrome animals leads to specific activation of the hippocampus, and deletion of $Na_V1.1$ in the hippocampus of functionally wild type mice gives them a subset of Dravet Syndrome symptoms: seizures and cognitive deficit.

These findings both deepen our understanding of the etiology of this devastating disease and provide a therapeutic target for future genetic manipulations.

4.6 Figure

Fig. 1: Using CRISPR/Cas to repair the R1407X mutation in a mouse model of Dravet Syndrome

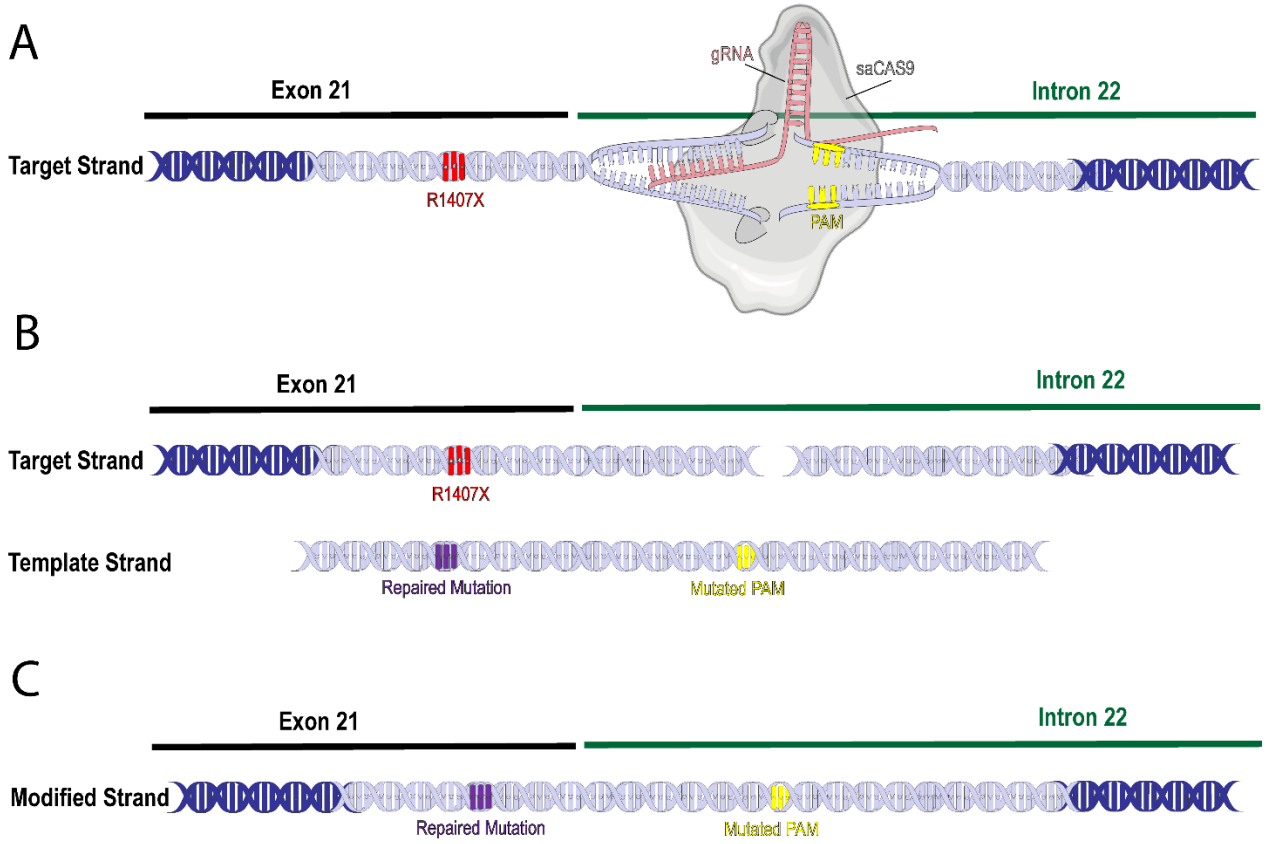

Schematic of hypothetical CRISPR/Cas experimental design to repair the R1407X mutation in Dravet mice. (A) Illustration of SaCas binding to guide RNA (gRNA) and cutting the DNA near the protospacer adjacent motif (PAM) in intron 22 located proximal to the exon 21 containing the R1407X mutation. (B) Schematic of template strand containing the repaired mutation, mutated PAM site, and the corresponding homology domain with the target strand. (C) Illustration of desired outcome, where template strand is inserted in a position where the repair sequence is integrated.

References

Barnes, C.A. (1979). Memory deficits associated with senescence: a neurophysiological and behavioral study in the rat. Journal of comparative and physiological psychology *93*, 74-104.

Bechi, G., Scalmani, P., Schiavon, E., Rusconi, R., Franceschetti, S., and Mantegazza, M. (2012). Pure haploinsufficiency for Dravet syndrome Na(V)1.1 (SCN1A) sodium channel truncating mutations. Epilepsia *53*, 87-100.

Becker, A.J., Pitsch, J., Sochivko, D., Opitz, T., Staniek, M., Chen, C.C., Campbell, K.P., Schoch, S., Yaari, Y., and Beck, H. (2008). Transcriptional upregulation of Cav3.2 mediates epileptogenesis in the pilocarpine model of epilepsy. J Neurosci *28*, 13341-13353.

Catterall, W.A. (2000). From ionic currents to molecular mechanisms: The structure and function of voltage-gated sodium channels. Neuron *26*, 13-25.

Catterall, W.A. (2014). Sodium channels, inherited epilepsy, and antiepileptic drugs. Annu Rev Pharmacol Toxicol *54*, 317-338.

Catterall, W.A. (2018). Dravet Syndrome: a sodium channel interneuronopathy. Curr Opin Physiol *2*, 42-50.

Catterall, W.A., Kalume, F., and Oakley, J.C. (2010a). $Na_V1.1$ channels and epilepsy. J Physiol *588*, 1849-1859.

Catterall, W.A., Kalume, F., and Oakley, J.C. (2010b). NaV1.1 channels and epilepsy. J Physiol *588*, 1849-1859.

Cheah, C.S., Westenbroek, R.E., Roden, W.H., Kalume, F., Oakley, J.C., Jansen, L.A., and Catterall, W.A. (2013). Correlations in timing of sodium channel expression, epilepsy, and sudden death in Dravet syndrome. Channels (Austin) *7*, 468-472.

Cheah, C.S., Yu, F.H., Westenbroek, R.E., Kalume, F.K., Oakley, J.C., Potter, G.B., Rubenstein, J.L., and Catterall, W.A. (2012). Specific deletion of NaV1.1 sodium channels in inhibitory interneurons causes seizures and premature death in a mouse model of Dravet syndrome. Proc Natl Acad Sci U S A *109*, 14646-14651.

Chiron, C., and Dulac, O. (2011). The pharmacologic treatment of Dravet syndrome. Epilepsia *52 Suppl 2*, 72-75.

Claes, L., Ceulemans, B., Audenaert, D., Smets, K., Lofgren, A., Del-Favero, J., Ala-Mello, S., Basel-Vanagaite, L., Plecko, B., Raskin, S.*, et al.* (2003). De novo SCN1A mutations are a major cause of severe myoclonic epilepsy of infancy. Hum Mutat *21*, 615-621.

Claes, L., Del-Favero, J., Ceulemans, B., Lagae, L., Van Broeckhoven, C., and De Jonghe, P. (2001). De novo mutations in the sodium-channel gene SCN1A cause severe myoclonic epilepsy of infancy. Am J Hum Genet *68*, 1327-1332.

Cooper, M.S., McIntosh, A., Crompton, D.E., McMahon, J.M., Schneider, A., Farrell, K., Ganesan, V., Gill, D., Kivity, S., Lerman-Sagie, T.*, et al.* (2016). Mortality in Dravet syndrome. Epilepsy Res *128*, 43-47.

Crandall, S.R., and Connors, B.W. (2016). Diverse Ensembles of Inhibitory Interneurons. Neuron *90*, 4-6.

Crawley, J.N. (1999). Behavioral phenotyping of transgenic and knockout mice: experimental design and evaluation of general health, sensory functions, motor abilities, and specific behavioral tests. Brain Res *835*, 18-26.

Deverman, B.E., Pravdo, P.L., Simpson, B.P., Kumar, S.R., Chan, K.Y., Banerjee, A., Wu, W.L., Yang, B., Huber, N., Pasca, S.P.*, et al.* (2016). Cre-dependent selection yields AAV variants for widespread gene transfer to the adult brain. Nat Biotechnol *34*, 204-209.

Devinsky, O., Cross, J.H., Laux, L., Marsh, E., Miller, I., Nabbout, R., Scheffer, I.E., Thiele, E.A., Wright, S., and Cannabidiol in Dravet Syndrome Study, G. (2017). Trial of Cannabidiol for Drug-Resistant Seizures in the Dravet Syndrome. N Engl J Med *376*, 2011-2020.

Dravet, C. (2011a). Dravet syndrome history. Dev Med Child Neurol *53 Suppl 2*, 1-6.

Dravet, C. (2011b). The core Dravet syndrome phenotype. Epilepsia *52 Suppl 2*, 3-9.

Dravet, C., Bureau, M., Oguni, H., Fukuyama, Y., and Cokar, O. (2005). Severe myoclonic epilepsy in infancy: Dravet syndrome. Adv Neurol *95*, 71-102.

Eichenbaum, H., Stewart, C., and Morris, R.G. (1990). Hippocampal representation in place learning. J Neurosci *10*, 3531-3542.

Engel, J. (1990). Functional explorations of the human epileptic brain and their therapeutic implications. Electroencephalography and Clinical Neurophysiology *76*.

Engel, J., Jr. (1996). Excitation and inhibition in epilepsy. Can J Neurol Sci *23*, 167-174.

Favero, M., Sotuyo, N.P., Lopez, E., Kearney, J.A., and Goldberg, E.M. (2018). A transient developmental window of fast-spiking interneuron dysfunction in a mouse model of Dravet Syndrome. J Neurosci *38*, 7912-7927.

Fisher, R.S., Cross, J.H., French, J.A., Higurashi, N., Hirsch, E., Jansen, F.E., Lagae, L., Moshe, S.L., Peltola, J., Roulet Perez, E.*, et al.* (2017). Operational classification of seizure types by the International League Against Epilepsy: Position Paper of the ILAE Commission for Classification and Terminology. Epilepsia *58*, 522-530.

Gaj, T., Epstein, B.E., and Schaffer, D.V. (2016). Genome Engineering Using Adeno-associated Virus: Basic and Clinical Research Applications. Molecular therapy : the journal of the American Society of Gene Therapy *24*, 458-464.

Gelman, D., Griveau, A., Dehorter, N., Teissier, A., Varela, C., Pla, R., Pierani, A., and Marín, O. (2011). A wide diversity of cortical GABAergic interneurons derives from the embryonic preoptic area. The Journal of Neuroscience *31*, 16570-16580.

Genton, P., Velizarova, R., and Dravet, C. (2011). Dravet syndrome: the long-term outcome. Epilepsia *52 Suppl 2*, 44-49.

Gore, B.B., Soden, M.E., and Zweifel, L.S. (2013). Manipulating gene expression in projection-specific neuronal populations using combinatorial viral approaches. Curr Protoc Neurosci *65*, 4 35 31-20.

Gschwind, M.A., and Seeck, M. (2016). Modern management of seizures and epilepsy. Swiss Medical Weekly *146*.

Guenthner, C.J., Miyamichi, K., Yang, H.H., Heller, H.C., and Luo, L. (2013). Permanent genetic access to transiently active neurons via TRAP: targeted recombination in active populations. Neuron *78*, 773-784.

Han, S., Tai, C., Westenbroek, R.E., Yu, F.H., Cheah, C.S., Potter, G.B., Rubenstein, J.L., Scheuer, T., de la Iglesia, H.O., and Catterall, W.A. (2012a). Autistic-like behaviour in *Scn1a*$^{+/-}$ mice and rescue by enhanced GABA-mediated neurotransmission. Nature *489*, 385-390.

Han, S., Yu, F.H., Schwartz, M.D., Linton, J.D., Bosma, M.M., Hurley, J.B., Catterall, W.A., and de la Iglesia, H.O. (2012b). $Na_V1.1$ channels are critical for intercellular communication in the suprachiasmatic nucleus and for normal circadian rhythms. Proc Natl Acad Sci U S A *109*, E368-377.

Hawkins, N.A., Anderson, L.L., Gertler, T.S., Laux, L., George, A.L., Jr., and Kearney, J.A. (2017). Screening of conventional anticonvulsants in a genetic mouse model of epilepsy. Ann Clin Transl Neurol *4*, 326-339.

Hedrich, U.B., Liautard, C., Kirschenbaum, D., Pofahl, M., Lavigne, J., Liu, Y., Theiss, S., Slotta, J., Escayg, A., Dihne, M.*, et al.* (2014). Impaired action potential initiation in GABAergic interneurons causes hyperexcitable networks in an epileptic mouse model carrying a human Na(V)1.1 mutation. J Neurosci *34*, 14874-14889.

Ito, S., Ogiwara, I., Yamada, K., Miyamoto, H., Hensch, T.K., Osawa, M., and Yamakawa, K. (2013a). Mouse with Nav1.1 haploinsufficiency, a model for Dravet syndrome, exhibits lowered sociability and learning impairment. Neurobiology of disease *49*, 29-40.

Ito, S., Ogiwara, I., Yamada, K., Miyamoto, H., Hensch, T.K., Osawa, M., and Yamakawa, K. (2013b). Mouse with Nav1.1 haploinsufficiency, a model for Dravet syndrome, exhibits lowered sociability and learning impairment. Neurobiol Dis *49*, 29-40.

Kalume, F., Oakley, J.C., Westenbroek, R.E., Gile, J., de la Iglesia, H.O., Scheuer, T., and Catterall, W.A. (2015). Sleep impairment and reduced interneuron excitability in a mouse model of Dravet Syndrome. Neurobiol Dis *77*, 141-154.

Kalume, F., Westenbroek, R.E., Cheah, C.S., Yu, F.H., Oakley, J.C., Scheuer, T., and Catterall, W.A. (2013a). Sudden unexpected death in a mouse model of Dravet syndrome. J Clin Invest *123*, 1798-1808.

Kalume, F., Westenbroek, R.E., Cheah, C.S., Yu, F.H., Oakley, J.C., Scheuer, T., and Catterall, W.A. (2013b). Sudden unexpected death in a mouse model of Dravet syndrome. The Journal of clinical investigation *123*, 1798-1808.

Kalume, F., Yu, F.H., Westenbroek, R.E., Scheuer, T., and Catterall, W.A. (2007). Reduced sodium current in Purkinje neurons from Nav1.1 mutant mice: implications for ataxia in severe myoclonic epilepsy in infancy. J Neurosci *27*, 11065-11074.

Kaplan, J.S., Stella, N., Catterall, W.A., and Westenbroek, R.E. (2017). Cannabidiol attenuates seizures and social deficits in a mouse model of Dravet syndrome. Proc Natl Acad Sci U S A *114*, 11229-11234.

Kelsom, C., and Lu, W. (2013). Development and Specification of GABAergic Cortical Interneurons. Cell and Bioscience.

Krook-Magnuson, E., Armstrong, C., Bui, A., Lew, S., Oijala, M., and Soltesz, I. (2015). In vivo evaluation of the dentate gate theory in epilepsy. J Physiol *593*, 2379-2388.

Krook-Magnuson, E., Szabo, G.G., Armstrong, C., Oijala, M., and Soltesz, I. (2014). Cerebellar directed optogenetic intervention inhibits spontaneous hippocampal seizures in a mouse model of temporal lobe epilepsy. eNeuro *1*.

Leo, A., Russo, E., and Elia, M. (2016). Cannabidiol and epilepsy: rationale and therapeutic potential. Pharmacol Res.

Lothman, E.W., Stringer, J.L., and Bertram, E.H. (1992). The dentate gyrus as a control point for seizures in the hippocampus and beyond. Epilepsy Res Suppl *7*, 301-313.

Luders, H. (2008). Textbook of Epilepsy Surgery (Informa Medical).

Manent, J.B., Beguin, S., Ganay, T., and Represa, A. (2011). Cell-autonomous and cell-to-cell signalling events in normal and altered neuronal migration. European Journal of Neuroscience *34*, 1595-1608.

Marini, C., Scheffer, I.E., Nabbout, R., Mei, D., Cox, K., Dibbens, L.M., McMahon, J.M., Iona, X., Carpintero, R.S., Elia, M.*, et al.* (2009). SCN1A duplications and deletions detected in Dravet syndrome: implications for molecular diagnosis. Epilepsia *50*, 1670-1678.

Marini, C., Scheffer, I.E., Nabbout, R., Suls, A., De Jonghe, P., Zara, F., and Guerrini, R. (2011). The genetics of Dravet syndrome. Epilepsia *52 Suppl 2*, 24-29.

Massaro, G., Mattar, C.N.Z., Wong, A.M.S., Sirka, E., Buckley, S.M.K., Herbert, B.R., Karlsson, S., Perocheau, D.P., Burke, D., Heales, S.*, et al.* (2018). Fetal gene therapy for neurodegenerative disease of infants. Nat Med *24*, 1317-1323.

Mistry, A.M., Thompson, C.H., Miller, A.R., Vanoye, C.G., George, A.L., Jr., and Kearney, J.A. (2014). Strain- and age-dependent hippocampal neuron sodium currents correlate with epilepsy severity in Dravet syndrome mice. Neurobiol Dis *65*, 1-11.

Morris, R.G., Garrud, P., Rawlins, J.N., and O'Keefe, J. (1982). Place navigation impaired in rats with hippocampal lesions. Nature *297*, 681-683.

Nabbout, R., Gennaro, E., Dalla Bernardina, B., Dulac, O., Madia, F., Bertini, E., Capovilla, G., Chiron, C., Cristofori, G., Elia, M.*, et al.* (2003). Spectrum of SCN1A mutations in severe myoclonic epilepsy of infancy. Neurology *60*, 1961-1967.

Oakley, J.C., Kalume, F., Yu, F.H., Scheuer, T., and Catterall, W.A. (2009). Temperature- and age-dependent seizures in a mouse model of severe myoclonic epilepsy in infancy. Proc Natl Acad Sci U S A *106*, 3994-3999.

Ogiwara, I., Iwasato, T., Miyamoto, H., Iwata, R., Yamagata, T., Mazaki, E., Yanagawa, Y., Tamamaki, N., Hensch, T.K., Itohara, S.*, et al.* (2013). Nav1.1 haploinsufficiency in excitatory neurons ameliorates seizure-associated sudden death in a mouse model of Dravet syndrome. Hum Mol Genet *22*, 4784-4804.

Ogiwara, I., Miyamoto, H., Morita, N., Atapour, N., Mazaki, E., Inoue, I., Takeuchi, T., Itohara, S., Yanagawa, Y., Obata, K.*, et al.* (2007). Nav1.1 localizes to axons of parvalbumin-positive inhibitory interneurons: a circuit basis for epileptic seizures in mice carrying an Scn1a gene mutation. J Neurosci *27*, 5903-5914.

Oguni, H., Hayashi, K., Osawa, M., Awaya, Y., Fukuyama, Y., Fukuma, G., Hirose, S., Mitsudome, A., and Kaneko, S. (2005). Severe myoclonic epilepsy in infancy: clinical analysis and relation to SCN1A mutations in a Japanese cohort. Advances in neurology *95*, 103-117.

Pearce, J.M. (2002). Bromide, the first effective antiepileptic agent. J Neurol Neurosurg Psychiatry *72*, 412.

Racine, R., Okujava, V., and Chipashvili, S. (1972). Modification of seizure activity by electrical stimulation. 3. Mechanisms. Electroencephalogr Clin Neurophysiol *32*, 295-299.

Ran, F.A., Cong, L., Yan, W.X., Scott, D.A., Gootenberg, J.S., Kriz, A.J., Zetsche, B., Shalem, O., Wu, X., Makarova, K.S.*, et al.* (2015). In vivo genome editing using Staphylococcus aureus Cas9. Nature *520*, 186-191.

Reid, J.M., Goetz, M.P., Buhrow, S.A., Walden, C., Safgren, S.L., Kuffel, M.J., Reinicke, K.E., Suman, V., Haluska, P., Hou, X.*, et al.* (2014). Pharmacokinetics of endoxifen and tamoxifen in female mice: implications for comparative in vivo activity studies. Cancer Chemother Pharmacol *74*, 1271-1278.

Richards, K.L., Milligan, C.J., Richardson, R.J., Jancovski, N., Grunnet, M., Jacobson, L.H., Undheim, E.A.B., Mobli, M., Chow, C.Y., Herzig, V.*, et al.* (2018). Selective NaV1.1 activation rescues Dravet syndrome mice from seizures and premature death. Proc Natl Acad Sci U S A *115*, E8077-E8085.

Rubinstein, M., Han, S., Tai, C., Westenbroek, R.E., Hunker, A., Scheuer, T., and Catterall, W.A. (2015a). Dissecting the phenotypes of Dravet syndrome by gene deletion. Brain *138*, 2219-2233.

Rubinstein, M., Westenbroek, R.E., Yu, F.H., Jones, C.J., Scheuer, T., and Catterall, W.A. (2015b). Genetic background modulates impaired excitability of inhibitory neurons in a mouse model of Dravet syndrome. Neurobiol Dis *73*, 106-117.

Rudy, B., Fishell, G., Lee, S., and Hjerling-Leffler, J. (2011). Three groups of interneurons account for nearly 100% of neocortical GABAergic neurons. Dev Neurobiol *71*, 45-61.

Sander, J.D., and Joung, J.K. (2014). CRISPR-Cas systems for editing, regulating and targeting genomes. Nature biotechnology *32*, 347-355.

Schutte, S.S., Schutte, R.J., Barragan, E.V., and O'Dowd, D.K. (2016). Model systems for studying cellular mechanisms of SCN1A related epilepsy. J Neurophysiol, jn 00824 02015.

Sheng, M., and Greenberg, M.E. (1990). The regulation and function of c-fos and other immediate early genes in the nervous system. Neuron *4*, 477-485.

Shorvon S, Guerrini R, Trinka E, and S, S. (2019). The Causes of Epilepsy: Diagnosis and Investigation (Cambridge University Press).

Stein, R.E., Kaplan, J.S., Li, J., and Catterall, W.A. (2019). Hippocampal deletion of NaV1.1 channels in mice causes thermal seizures and cognitive deficit characteristic of Dravet Syndrome. Proc Natl Acad Sci U S A *116*, 16571-16576.

Tai, C., Abe, Y., Westenbroek, R.E., Scheuer, T., and Catterall, W.A. (2014). Impaired excitability of somatostatin- and parvalbumin-expressing cortical interneurons in a mouse model of Dravet syndrome. Proc Natl Acad Sci U S A *111*, E3139-3148.

Tatsukawa, T., Ogiwara, I., Mazaki, E., Shimohata, A., and Yamakawa, K. (2018a). Impairments in social novelty recognition and spatial memory in mice with conditional deletion of *Scn1a* in parvalbumin-expressing cells. Neurobiol Dis *112*, 24-34.

Tatsukawa, T., Ogiwara, I., Mazaki, E., Shimohata, A., and Yamakawa, K. (2018b). Impairments in social novelty recognition and spatial memory in mice with conditional deletion of Scn1a in parvalbumin-expressing cells. Neurobiology of disease *112*, 24-34.

Temkin, O. (1945). The falling sickness; a history of epilepsy from the Greeks to the beginnings of modern neurology (Baltimore,: The Johns Hopkins Press).

Trimmer, J.S. (1998). Regulation of ion channel expression by cytoplasmic subunits. CurrOpinNeurobiol *8*, 370-374.

Vann, S.D., and Albasser, M.M. (2011). Hippocampus and neocortex: recognition and spatial memory. Curr Opin Neurobiol *21*, 440-445.

Westenbroek, R.E., Merrick, D.K., and Catterall, W.A. (1989). Differential subcellular localization of the RI and RII Na+ channel subtypes in central neurons. Neuron *3*, 695-704.

Winters, B.D., Forwood, S.E., Cowell, R.A., Saksida, L.M., and Bussey, T.J. (2004). Double dissociation between the effects of peri-postrhinal cortex and hippocampal lesions on tests of object recognition and spatial memory: heterogeneity of function within the temporal lobe. J Neurosci *24*, 5901-5908.

Xiao-Jie, L., Hui-Ying, X., Zun-Ping, K., Jin-Lian, C., and Li-Juan, J. (2015). CRISPR-Cas9: a new and promising player in gene therapy. Journal of medical genetics *52*, 289-296.

Yang, H., Shan, W., Zhu, F., Yu, T., Fan, J., Guo, A., Li, F., Yang, X., and Wang, Q. (2019). C-Fos mapping and EEG characteristics of multiple mice brain regions in pentylenetetrazol-induced seizure mice model. Neurol Res, 1-13.

Yu, F.H., Mantegazza, M., Westenbroek, R.E., Robbins, C.A., Kalume, F., Burton, K.A., Spain, W.J., McKnight, G.S., Scheuer, T., and Catterall, W.A. (2006). Reduced sodium current in GABAergic interneurons in a mouse model of severe myoclonic epilepsy in infancy. Nat Neurosci *9*, 1142-1149.

Yu, L.M., Polygalov, D., Wintzer, M.E., Chiang, M.C., and McHugh, T.J. (2016). CA3 Synaptic Silencing Attenuates Kainic Acid-Induced Seizures and Hippocampal Network Oscillations. eNeuro *3*.